

Field Theory of Compact Polymers on the Square Lattice

Jesper Lykke Jacobsen^{1,2,*} and Jané Kondev^{3,4,†}

¹*Somerville College and Department of Theoretical Physics, University of Oxford, 1 Keble Road, Oxford OX1 3NP, U.K.*

²*Institute of Physics and Astronomy, University of Aarhus, Ny Munkegade, DK-8000 Aarhus C, Denmark.*

³*Institute for Advanced Study, Olden Lane, Princeton, NJ 08540.*

⁴*Department of Physics, Princeton University, Princeton, NJ 08540.*

(June 25, 2018)

Exact results for conformational statistics of compact polymers are derived from the two-flavour fully packed loop model on the square lattice. This loop model exhibits a *two-dimensional manifold* of critical fixed points each one characterised by an infinite set of geometrical scaling dimensions. We calculate these dimensions *exactly* by mapping the loop model to an interface model whose scaling limit is described by a Liouville field theory. The formulae for the central charge and the first few scaling dimensions are compared to numerical transfer matrix results and excellent agreement is found. Compact polymers are identified with a particular point in the phase diagram of the loop model, and the non-mean field value of the conformational exponent $\gamma = 117/112$ is calculated for the first time. Interacting compact polymers are described by a *line* of fixed points along which γ varies continuously.

PACS numbers: 05.50.+q, 11.25.Hf, 64.60.Ak, 64.60.Fr

I. INTRODUCTION

Lattice models of loops have emerged as an important paradigm in two-dimensional critical phenomena. They allow for a determination of the scaling properties of different types of random walks which are used to model conformations of different phases of polymers [1]. For instance, the solution of the $O(n)$ loop model has led to exact results for conformational exponents of swollen and dense polymers [2], as well as polymers at the theta point [3]. The theta point is the tricritical point which governs the transition between the swollen and the collapsed phase of polymers in solution [1]. Examples of conformational exponents are γ , which describes the scaling of the number of polymer conformations with the number of monomers \mathcal{N} , and ν , for the scaling of the linear size of a polymer, as measured by the radius of gyration, with \mathcal{N} . Here we calculate for the first time the exact value of γ for polymers on the square lattice, in the *compact phase*. Compact polymers completely fill the lattice and are of direct relevance to statistical studies of protein folding [4,5].

Further motivation for studying loop models comes from the Fortuin-Kasteleyn construction which maps many discrete spin models (e.g., Q -state Potts) to random cluster models. Since cluster boundaries in two dimensions form loops this naturally leads to a loop model representation. This random geometrical description of two-dimensional lattice models then provides a setting in which a general theory of their scaling limits can be

sought. It is one of the goals of this paper to outline a specific proposal for such a theory in the form of an effective field theory of fluctuating loops. This field theory is constructed following the Coulomb gas recipe [6] with some important new ingredients added [7]. It describes the fluctuations of a random surface for which the loops are contour lines.

Scaling limits of many (but not all) two-dimensional lattice models are described by conformally invariant field theories [8,9]. This observation has led to exact results for critical exponents and other universal quantities, and to a classification of critical points based on their symmetry properties with respect to the group of conformal transformations. An obvious question which is often difficult to answer is: given a particular lattice model how does one *construct* the conformal field theory of its scaling limit? Loop models provide examples for which the scaling limit can be constructed in a *physically* transparent way. This is accomplished by mapping a loop model to an interface model, where the loops are simply equal-height contours. An explicit coarse graining procedure is then implemented for the height model, and it leads to a well known conformal field theory – the *Liouville field theory*.

Interesting examples of loop models are also provided by one-dimensional quantum models, spin chains in particular, where loops appear as world lines of the spin. This mapping of spins to loops has recently been used to formulate very efficient numerical schemes for simulating spin chains and ladders. These *loop algorithms* al-

*E-mail: lykke@dfi.aau.dk ; lykke@thphys.ox.ac.uk

†E-mail: janek@ias.edu

low one to simulate much bigger system sizes and lower temperatures than by using more traditional algorithms with local updates [10]. The loop representation of quantum spin chains also gives an illuminating stochastic-geometrical view of their quantum fluctuations [11]. For example, the spin-spin correlation function is related to the probability that two points on the space-time lattice belong to the same loop. This insight might lead to a *practical* theory of plateau transitions in the Integer Quantum Hall Effect, i. e., one that would allow for a calculation of the correlation length exponent and other universal quantities which have been measured in experiments. Namely, the Chalker-Coddington network model [12], which is believed to be in the same universality class as the plateau transitions, was recently mapped to an $SU(n \rightarrow 0)$ quantum spin chain [13]. It remains to be seen if this spin chain has a tractable loop-model representation.

In the bigger picture, loop models are of interest as simple examples where the fundamental constituents are non-local, extended objects as opposed to point-like objects such as particles and spins. Fluctuating geometries of this sort are used to model flux lines in superconductors, domain walls in magnets, and crystalline interfaces, to name a few experimentally relevant systems.

The extended nature of loops turns out to have profound consequences when one attempts to write down an effective continuum description of these models, say, following Landau’s dictum of expanding the free energy (Euclidean action) in powers of the order parameter and its derivatives. Namely, terms which are geometrical in origin and non-perturbative in nature, and hence cannot be inferred from symmetry arguments alone, appear in the action. On the other hand, exactly *because* these geometrical terms are present the values of the *effective* coupling constants of the field theory are completely determined, a rather remarkable occurrence.

Usually in an effective description provided by a field theory, coupling constants are phenomenological parameters fixed by auxiliary information about observable quantities, such as the response functions or the related correlation functions. The Coulomb gas approach to two-dimensional critical phenomena is an example of an effective theory wherein the electromagnetic coupling constant (i. e., the “magnitude of the unit charge”) is determined from an exact solution of the model; typically it suffices to calculate the exact value of a single critical exponent. Our construction of an effective field theory of loop models closely parallels the Coulomb gas method with the important difference that the coupling constants are determined without recourse to any exact information about the model. For the model at hand no such information is available anyway, and moreover there are indications that the model is not exactly solvable [14]. On one level our theory can be viewed as a trick that allows one to calculate critical exponents in two-dimensional loop

models without doing the “hard work” of exactly solving the model. On a deeper level it shows that lattice models of loops lead to continuum theories that are *geometrical* in nature, i. e., devoid of any couplings that depend on the microscopic details.

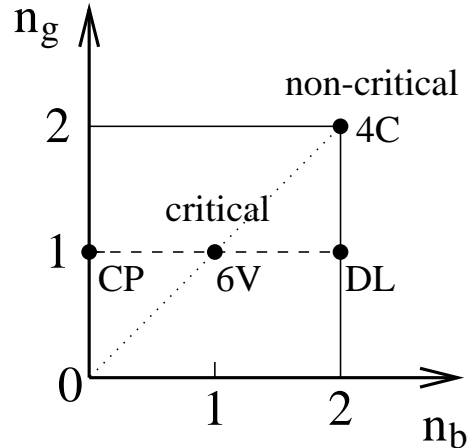


FIG. 1. Phase diagram of the two-flavour fully packed loop model on the square lattice. The loop model is critical for loop fugacities $0 \leq n_b, n_g \leq 2$. Particular points in the critical phase map to previously studied models: 6V – equal weighted six-vertex model [16], DL – dimer loop model [15], 4C – four-colouring model [28]. The dashed line is the fully packed loop model studied numerically in Ref. [14]; the point CP along this line corresponds to the problem of compact polymers. Finally, the dotted line is the loop model for which an effective Liouville field theory was constructed in Ref. [7].

Here we study in detail the two-flavour fully packed loop (FPL²) model on the square lattice. This is a statistical model which describes two flavours of loops that occupy the bonds of the square lattice, subject to certain close packing constraints to which we shall return shortly. The phase diagram of this model is described by two variables, n_b and n_g , which are the loop fugacities of the two flavours; see Fig. 1. The phase diagram of the FPL² model has three important features that we wish to emphasize from the outset:

- i) For loop fugacities that fall into the region $0 \leq n_b, n_g \leq 2$ of the phase diagram the model is critical, i. e., it exhibits a power-law distribution of loop sizes. The novel feature is that every point in the critical region defines a *different* universality class characterised by an infinite set of geometrical critical exponents. All previously studied loop models (e.g., Q -state Potts, $O(n)$ models) exhibit a *line* of fixed points.
- ii) The effective field theory of the FPL² model in the critical region describes a fluctuating two-dimensional interface in five dimensions, which is characterised by *three* elastic constants. We calculate these three couplings exactly as a function of the two loop fugacities. It is important to note that all previously solved loop models are

characterised by a single elastic constant.

iii) From the field theory of the FPL² model we calculate for the first time *exact* results for the conformational exponents of compact polymers on the square lattice. Furthermore, a particular line of fixed points in the phase diagram of the FPL² model can be identified with *interacting* compact polymers ($n_b = 0, n_g \leq 2$). We find that along this line the exponent γ changes continuously, whilst ν stays constant.

The organisation of the paper is as follows. In Sec. II we review the scaling theory of compact polymers which provides our main motivation for introducing the two-flavour fully packed loop model on the square lattice in Sec. III. The rest of the paper is devoted to the study of this model using field theoretical techniques and numerical transfer matrix calculations.

The FPL² model is mapped to an interface model in Sec. IV. For the interface model we construct the scaling limit in terms of a Liouville field theory, in Sec. V. In Secs. VI and VII we make use of the field theory to calculate the central charge and the infinite set of geometrical exponents associated with loops, in the critical region of the loop model. A short description of the non-critical region based on the field theory is given next in Sec. VIII.

Following the field theoretical treatment of the FPL² model, in Secs. IX and X we describe the construction of transfer matrices for different boundary conditions. They are used to determine the central charge, the first few geometrical exponents, and the residual entropy; the numerical results are in excellent agreement with the theoretical predictions. Finally, in Sec. XI, we present some general observations regarding compact polymers and the Coulomb gas description of conformal field theories. We also comment on the dimer-loop model [15] and the three-state Potts antiferromagnet [16], in light of our solution of the fully packed loop model on the square lattice. The appendices are reserved for the calculation of scaling dimensions of operators in the Liouville field theory and the enumeration of connectivities which are used for constructing the transfer matrices.

II. COMPACT POLYMERS

Compact polymers, or Hamiltonian walks, are self-avoiding random walks that visit *all* the sites of the underlying lattice; see Fig. 2. They have been used as simple models of polymer melts [17] and appear in statistical studies of protein folding [4,5]. Unlike dilute and

dense polymers whose scaling properties were calculated exactly from the $O(n)$ loop model [18], compact polymers defied a similar treatment until recently. Numerical transfer matrix calculations [19], a Bethe-ansatz solution [20], and a Coulomb gas theory [21] of the fully packed loop model on the *honeycomb* lattice, all conclude that compact polymers define a new universality class of critical behaviour. Here we study compact polymers on the *square* lattice. We calculate exact scaling exponents and find them to be distinct from the honeycomb case. This was first reported in Ref. [14] on the basis of numerical transfer matrix results.

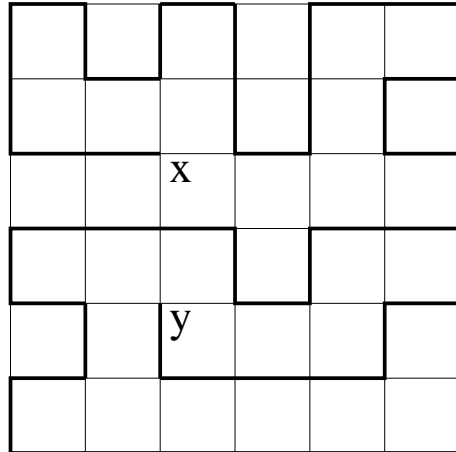


FIG. 2. Compact polymer on the square lattice; x and y are the positions of the chain ends.

The lattice dependence of critical properties distinguishes the compact polymer problem from its dilute and dense counterparts in a crucial way. It places them into the class of geometrically frustrated critical systems¹. A physically relevant measure of frustration for compact polymers is the number of *contacts* per monomer. Contacts are realised by monomer pairs where the two monomers are nearest neighbors on the lattice but are not adjacent along the polymer chain. In lattice models of proteins hydrophobic interactions among the amino acids occur at contacts [4,5]. For the square model studied here the number of contacts per monomer is *two*, whilst on the honeycomb lattice it is *one*.

In order to study the scaling properties of compact polymers we focus our attention on the two most widely studied conformational exponents ν and γ . If R is the radius of gyration of the polymer then

$$R \sim \mathcal{N}^\nu, \quad (2.1)$$

¹Another example is the antiferromagnetic three-state Potts model which has a zero-temperature critical point on the square [16] and the Kagomé [22] lattices characterised by different critical exponents.

where \mathcal{N} is the number of monomers. Since compact polymers visit all the sites of a lattice, they are space-filling and we conclude that $\nu = 1/2$. This simple result will serve as an important check on our field theoretical calculations where it will be recovered.

In order to define the conformational exponent γ we introduce $C(\mathcal{N})$, the number of compact polymers (Hamiltonian walks) on a square lattice with \mathcal{N} sites. Since a compact polymer fills the lattice, boundary conditions (free, periodic, etc.) play an important rôle. Following Saleur and Duplantier [23], we define γ in a way that is insensitive to the boundaries. Namely, if we introduce the quantity $C_o(\mathcal{N})$, the number of compact-polymer *rings*, then we can expect

$$\frac{C(\mathcal{N})}{C_o(\mathcal{N})} \sim \mathcal{N}^\gamma, \quad (2.2)$$

where γ does not depend on the choice of boundary conditions. Therefore, in order to calculate γ we need to solve the hard combinatorial problem of counting the number of open and closed compact polymers on the square lattice. Following de Gennes we do this by mapping the counting problem to the calculation of a correlation function in a particular statistical model at the critical point.

Consider the quantity $Z(\mathbf{x}, \mathbf{y}; \mathcal{N})$, the number of compact polymer conformations that start at the vertex \mathbf{x} of the $\sqrt{\mathcal{N}} \times \sqrt{\mathcal{N}}$ square lattice, and end at \mathbf{y} (see Fig. 2); we consider the limit $1 \ll |\mathbf{x} - \mathbf{y}| \ll \sqrt{\mathcal{N}}$, where \mathbf{x} and \mathbf{y} are chosen far from the boundaries of the lattice. For this quantity we can write down the scaling form [23]:

$$Z(\mathbf{x}, \mathbf{y}; \mathcal{N}) = C_o(\mathcal{N}) |\mathbf{x} - \mathbf{y}|^{-2x_1} f\left(\frac{|\mathbf{x} - \mathbf{y}|}{\mathcal{N}^{1/2}}\right), \quad (2.3)$$

where $f(u)$ is a scaling function with the property $f(u) \rightarrow \text{const.}$ as $u \rightarrow 0$, and x_1 is a geometrical exponent related to γ . Integrating $Z(\mathbf{x}, \mathbf{y}; \mathcal{N})$ over all end-points \mathbf{y} and comparing the result to Eq. (2.2), the scaling relation

$$\gamma = 1 - x_1 \quad (2.4)$$

follows.

To calculate the geometrical exponent x_1 we introduce the two-flavour fully packed loop model on the square lattice. The fact that we need *two* loop flavours follows from the simple observation that the bonds not covered by the compact polymer also form loops whose number is *unconstrained*. For the loop model we then construct an effective field theory in which $Z(\mathbf{x}, \mathbf{y}; \mathcal{N})$ becomes a two-point correlation function. The asymptotics of this function can be calculated exactly and we find $x_1 = -5/112$, from which

$$\gamma = 117/112 = 1.0446 \dots \quad (2.5)$$

follows. This is to be compared to the mean-field theory value $\gamma_{\text{MF}} = 1$ [24], which is also the result obtained for compact polymers on the honeycomb lattice [20].

The conformational exponent γ was measured directly from enumerations of conformations of chains with lengths up to 30 in Ref. [4], and the value $\gamma = 1.01(5)$ was reported. More recently, from a numerical transfer matrix study of the fully packed loop model on the square lattice the geometrical exponent $x_1 = -0.0444(1)$ was determined [14], in excellent agreement with the exact result.

Another quantity of interest is the connective constant κ which determines the leading, exponential with system size scaling of the number of compact polymers [25]

$$C(\mathcal{N}) \sim \kappa^{\mathcal{N}} \kappa_s^{\mathcal{N}^{(d-1)/d}} \mathcal{N}^{\gamma-1}. \quad (2.6)$$

Here κ_s is the surface connective constant; it appears due to the space-filling nature of compact polymers. Both the value $\kappa = 1.475(15)$ found in Ref. [4], and the estimate $\kappa \simeq 1.472$ obtained from transfer matrix calculations similar to ours [26], seem in favour of the mean-field result $\kappa_{\text{MF}} = \frac{4}{e} = 1.4715 \dots$ [24].² In Sec. XD we report the very accurate numerical value

$$\kappa = 1.472801(10), \quad (2.7)$$

which shows that the connective constant for compact polymers also deviates slightly from the mean-field result.

For the remainder of the paper we elaborate on the calculation of γ for compact polymers, in the process unveiling an extremely rich phase diagram of the associated loop model. As remarked earlier, it contains a two-dimensional region of fixed points, which we characterise in detail by calculating the central charge and the geometrical exponents associated with loops for each point on the critical manifold.

III. TWO-FLAVOUR LOOP MODEL

The two-flavour fully packed loop model on the square lattice was introduced in Ref. [28] as the loop representation of the four-colouring model [29]. It is the natural generalisation of the fully packed loop model on the honeycomb lattice, which is the loop representation of the three-colouring model [21]. In general, a q -colouring model on a q -fold coordinated lattice is given

²Very recently the field theory of Ref. [24] has been improved [27] yielding, however, unchanged values for γ_{MF} and κ_{MF} .

by edge colourings of the lattice with q different colours; an edge colouring of a graph is one where no two bonds that share a common vertex are coloured equally. The colouring model is mapped to a loop model by choosing $[q/2]$ colour-pairs; each pair defines strings of alternating colour that necessarily form loops (unless they terminate at the boundary). In this way we end up with a loop model with $[q/2]$ flavours of loops.

To define the FPL² model we first specify the allowed loop configurations \mathcal{G} . In \mathcal{G} every bond of the square lattice belongs to one and only one loop of either flavour, and loops of the same flavour are not allowed to cross. Representing the two flavours by solid (black) and hatched (grey) line segments respectively this fully packing constraint allows each vertex of the square lattice to have one of the six appearances depicted in Fig. 3. Each loop is assigned a fugacity depending on its flavour: n_b for black loops and n_g for grey loops. The partition function of the FPL² model is then

$$Z = \sum_{\mathcal{G}} n_b^{N_b} n_g^{N_g}. \quad (3.1)$$

The fully packed loop model of Batchelor *et al.* [14] is obtained by setting the loop fugacity of the grey loops to unity. In the limit $n_b \rightarrow 0$ we recover the compact polymer problem.

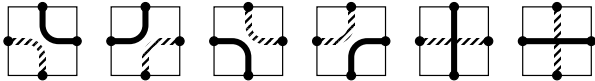


FIG. 3. The six vertex configurations of the FPL² model that are allowed by the fully packing constraint. Black and grey loop segments are shown here as solid and hatched lines respectively. Each vertex is adjacent to four edges, here shown as dots, that are referred to as “dangling” if they are not connected to an edge of a neighbouring vertex. Note that the two rightmost vertices explicitly permit the two flavours to cross.

If we define a restricted partition function of the FPL² model, to which only configurations with a single black loop segment propagating between points \mathbf{x} and \mathbf{y} contribute, then $Z(\mathbf{x}, \mathbf{y}; \mathcal{N})$ in Eq. (2.3) is obtained in the limit $n_b \rightarrow 0$, $n_g \rightarrow 1$. The first limit discards all configurations with black loops present, leaving only the black Hamiltonian walk (compact polymer) between \mathbf{x} and \mathbf{y} , whilst the second ensures that all walks are weighted equally. We could also consider weighting different Hamiltonian walks differently by setting $n_g \neq 1$. This situation can be interpreted as describing interacting compact polymers, and, as will be shown later, it leads to a continuously varying exponent γ . A similar property of interacting oriented polymers in the swollen phase was suggested by Cardy from a field theoretical

calculation [30]. Recent numerical studies of the interacting oriented self-avoiding walk by Trovato and Seno [31], though, seem to be at odds with Cardy’s prediction of an exponent γ that varies continuously with the interaction strength.

Some idea of the phase diagram of the FPL² model as a function of n_b and n_g can be gotten by examining the extreme limits of the loop fugacities. Namely, for $n_b, n_g \rightarrow \infty$ all loops have the minimum length of four, i.e., they each surround a single plaquette of the square lattice. There are no large loops in the system and the model is non-critical, or in other words, the average loop length is finite. On the other hand, in the critical phase of the loop model, which is the subject of this paper, in a typical configuration one finds loops of all sizes characterised by a power-law distribution. This leads to an average loop length which diverges with the system size. Such is the case in the other extreme limit of loop fugacities, $n_b, n_g \rightarrow 0$, when the loops cover the whole lattice.

Other previously studied models that are particular points in the phase diagram of the FPL² model are the four-colouring model, the dimer loop model, and the equal weighted six-vertex model; see Fig. 1. For $(n_b, n_g) = (2, 2)$ the loop fugacity of each loop can be evenly (1+1) distributed among the two ways of colouring the bonds occupied by the loop with two colours in an alternating fashion: **ABAB**... for black loops and **CDCD**... for grey loops. This is then the symmetric four-colouring model (**A, B, C,** and **D** are the colours) studied by Baxter [32]. In the dimer loop model black and white dimers are placed on the square lattice so that every vertex is covered by one of each [15]. If we identify the dimer covered bonds with the black loops then this model is mapped to the $(n_b, n_g) = (2, 1)$ FPL² model. And finally $(n_b, n_g) = (1, 1)$ constitutes the equal-weighted six-vertex model [33], the allowed vertices being those of Fig. 3.

IV. HEIGHT REPRESENTATION

The critical phase of the FPL² model can be described in terms of an effective field theory, following the general procedure discussed in Ref. [6]. The idea is to think of loops as contours of a scalar field, which we refer to as the height. Depending on the loop model in question the height can have one or more components. If the number of components is D_{\perp} then the effective field theory of the loop model describes a fluctuating two-dimensional interface in $D_{\perp} + 2$ dimensions.

To introduce the heights we first map the loop model to an *oriented* loop model, as shown in Fig. 4. The orientation of every loop is chosen randomly and independently. Every non-oriented loop configuration is thus transformed into an oriented one (\mathcal{G}'); the number of

oriented configurations that correspond to the same non-oriented loop configuration is simply $2^{N_b+N_g}$.

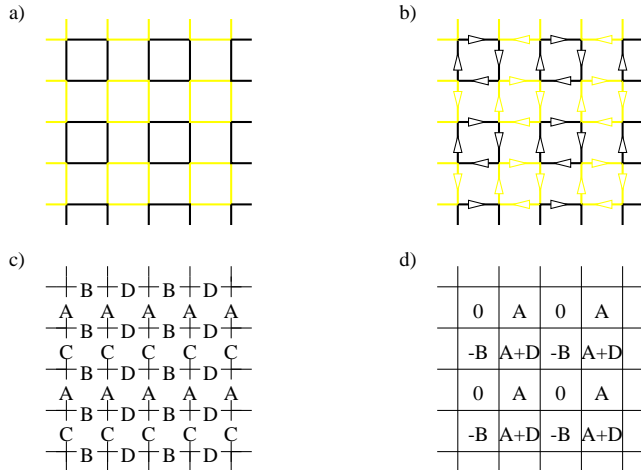


FIG. 4. Mapping of the FPL² model to an interface model. (a) \rightarrow (b): Transform the loop configuration into an *oriented* loop configuration by choosing the orientation of each loop independently and randomly. (b) \rightarrow (c): Every bond in the oriented loop configuration is in one of four states, depending on its flavour and direction; these four states are represented by three-vectors $\mathbf{A}, \mathbf{B}, \mathbf{C}$, and \mathbf{D} . (c) \rightarrow (d): The microscopic height \mathbf{z} of the interface model changes from plaquette to neighbouring plaquette by $\mathbf{A}, \mathbf{B}, \mathbf{C}$, or \mathbf{D} depending on the state of the bond between the two plaquettes. The change in \mathbf{z} is positive going clockwise around even vertices and counterclockwise around odd ones.

Next, for each loop we redistribute its weight (fugacity), n_b or n_g depending on whether it is black or grey, between the two possible orientations. For the black loops we do this by assigning to, say, the clockwise orientation the *phase factor* $\exp(i\pi e_b)$, and the opposite phase, $\exp(-i\pi e_b)$, to a counter-clockwise oriented black loop. Similarly for grey loops the clockwise oriented ones are assigned a weight $\exp(i\pi e_g)$ whilst the counter-clockwise loops are weighted with $\exp(-i\pi e_g)$. The loop fugacities are related to the newly introduced parameters e_b and e_g by

$$\begin{aligned} n_b &= 2 \cos(\pi e_b) \\ n_g &= 2 \cos(\pi e_g) \end{aligned} \quad (4.1)$$

since the partition function of the original (non-oriented) model, as given by Eq. (3.1), must be recovered by independently summing over the two possible orientations for each loop. Note that for $0 \leq n_b, n_g \leq 2$ the parameters e_b and e_g are real, whilst for $n_b, n_g > 2$ they are purely imaginary. As discussed in more detail in Sec. VIII this is the crucial property that leads to a critical state of the loop model in the former and a non-critical one in the latter case.

Now that the loops are oriented we can interpret them as contours of a height field; the orientation is necessary

as it determines the direction of increasing height. The systematic construction of the *microscopic heights* sets out from the observation that every bond of the square lattice is in one of four possible states: it can be coloured black or grey, and oriented from an even to an odd site, or from odd to even. “Even” and “odd” refer here to the two sublattices of the bipartite square lattice; every even site is surrounded by four nearest neighbouring odd sites, and *vice versa*.

The four possible bond-states are represented by four vectors – which are the colours in the four-colouring representation – $\mathbf{A}, \mathbf{B}, \mathbf{C}$ and \mathbf{D} ; see Fig. 4c. The microscopic heights $\{\mathbf{z}\}$ are defined on the dual lattice and the change in height when going from one plaquette centre to the next is given by $\mathbf{A}, \mathbf{B}, \mathbf{C}$ or \mathbf{D} , depending on the state of the bond which is crossed; Fig. 4d. For the height to be uniquely defined the four vectors must satisfy the constraint $\mathbf{A} + \mathbf{B} + \mathbf{C} + \mathbf{D} = 0$. This means that the microscopic heights live in a *three-dimensional* vector space, which we take to be \mathbf{Z}^3 . In other words the oriented FPL² model maps to a model of a two-dimensional interface in five spatial dimensions.

By reasons of symmetry the four vectors are chosen so as to point from the centre to the vertices of a regular tetrahedron. With a suitable choice of coordinates they are represented by three-vectors:

$$\begin{aligned} \mathbf{A} &= (-1, +1, +1) \\ \mathbf{B} &= (+1, +1, -1) \\ \mathbf{C} &= (-1, -1, -1) \\ \mathbf{D} &= (+1, -1, +1) . \end{aligned} \quad (4.2)$$

This is the same normalisation as the one used in Ref. [28].

Mapping the loop model to an oriented loop model also allows for a *local* redistribution of the loop weights. This is important since it leads to a local field theory for the heights. As we will find out shortly, though local, this field theory is somewhat unconventional due to the non-local, extended nature of the fundamental microscopic objects it purports to describe.

To redistribute the phase factors associated with oriented loops we assign a phase $\exp(-i\pi e_b/4)$ to a vertex of the square lattice if a black loop makes a left turn at that vertex, the opposite phase $\exp(+i\pi e_b/4)$ if it makes a right turn, and the weight 1 if it continues straight. The total vertex weight $\lambda(\mathbf{x})$ is a product of the phase factor originating from the black loop and an equivalent one from the grey loop passing through the same vertex \mathbf{x} . The partition function of the FPL² model, Eq. (3.1), can now be rewritten as a sum over oriented loop configurations (i.e., colouring configurations)

$$Z = \sum_{\mathcal{G}'} \prod_{\mathbf{x}} \lambda(\mathbf{x}) . \quad (4.3)$$

Once the height at a single point is fixed \mathcal{G}' is in a one-to-one correspondence with the configurations of the microscopic heights, and the summand in the above equation is the appropriate weight. In the critical phase of the FPL² model the interface described by Eq. (4.3) is *rough*, and the field theory is constructed so as to correctly reproduce its long-wavelength fluctuations.

A. Spectrum of electromagnetic charges

The mapping from oriented loop configurations, which are equivalent to edge colourings, to microscopic height configurations is one to many. In particular, two height configurations corresponding to the same edge colouring can have their heights shifted with respect to each other by a *global* shift $\mathbf{m} \in \mathcal{R}$. The set \mathcal{R} forms a three-dimensional Bravais lattice, i.e., it is closed under integral linear combinations, and its elements are the *magnetic* charges in the Coulomb gas representation of the FPL² model. The lattice reciprocal to the lattice of magnetic charges, \mathcal{R}^* , defines the *electric* charges $\mathbf{e} \in \mathcal{R}^*$, with the property $\mathbf{e} \cdot \mathbf{m} = 2\pi m$, $m \in \mathbf{Z}$.

The construction of the lattice \mathcal{R} for the FPL² model follows the usual prescription for height models, and has been carried out in detail in Ref. [28]. For the sake of completeness we outline this construction below.

It is convenient to first identify the *flat* states (also referred to as the *ideal* states), i.e., those colouring states which minimise the variance of the microscopic height \mathbf{z} . From the height mapping described above it follows that these states have all of their plaquettes coloured with two colours only; an example is shown in Fig. 4c. This leads to a colouring state that is periodic, with the same 2×2 colouring pattern repeated throughout the lattice. There are twenty four flat/ideal states for the colouring representation of the FPL² model, corresponding to the number of permutations of four different colours. Namely, an ideal state is completely specified by listing the colours of the bonds around a single site (say the origin), starting from the left horizontal bond and proceeding clockwise. To each flat state we assign a *coarse grained height* $\mathbf{h} = \langle \mathbf{z} \rangle$, which is the average microscopic height over a 2×2 unit cell of the colouring.

The flat states form a three dimensional graph, which we refer to as the ideal state graph, \mathcal{I} . Namely, starting from any ideal state four other ideal states can be reached by exchanging a pair of colours that form a plaquette. For example, by exchanging the colours **A** and **B** in Fig. 4c all the **ABAB** plaquettes are turned into **BABA** plaquettes to give a new ideal state. Under these plaquette flips only the microscopic heights at the centres of the affected plaquettes are changed. In this way the ideal states form a four-fold coordinated graph in height space, where each vertex is indexed by a colour permutation, and its position in \mathbb{R}^3 is given by the coarse grained

height \mathbf{h} . Bonds are associated with transpositions of two colours; they lie along the direction defined by the difference of the two colour vectors, and have a length of $\sqrt{2}/2$ if the normalisation in Eq. (4.2) is chosen.

The ideal state graph is a tiling of \mathbb{R}^3 with truncated octahedra; this regular polyhedron is better known as the Wigner-Seitz cell of a body-centred cubic (bcc) lattice (see Fig. 5). A single truncated octahedron in \mathcal{I} has twenty four vertices corresponding to the twenty four different ideal states. The set of vertices in \mathcal{I} representing the same ideal state form the *repeat lattice* \mathcal{R} , which is face-centred cubic (fcc) with a conventional cubic cell of side 4.

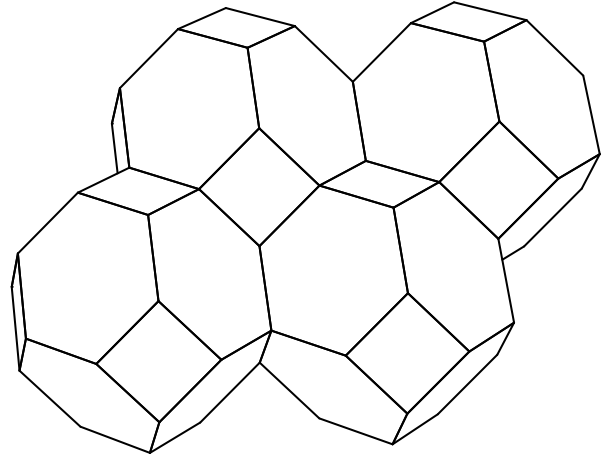


FIG. 5. The ideal state graph of the FPL² model in the four-colouring representation.

To obtain the continuum description of the FPL² model we coarse grain the microscopic height over domains of ideal states. This gives rise to the coarse grained height \mathbf{h} which we can consider to be *compactified* on \mathbb{R}^3/\mathcal{R} . The phase space of the height is not simply connected, thus allowing for topological defects (vortices) with topological charges that take their values in \mathcal{R} [34]. These defects are associated with *magnetic* charges in the Coulomb gas representation of the FPL² model. *Electric* charges on the other hand are associated with vertex operators $\exp(i\mathbf{e} \cdot \mathbf{h})$. If we take the height to live in \mathbb{R}^3/\mathcal{R} then vertex operators are well defined only for values of the electric charge $\mathbf{e} \in \mathcal{R}^*$. \mathcal{R}^* is the lattice *reciprocal* to the lattice of magnetic charges \mathcal{R} , and it is a body-centred cubic (bcc) lattice with a conventional cubic cell of side π .

V. CONSTRUCTION OF THE FIELD THEORY

An effective field theory of the FPL² model should describe large scale properties of loops. The kind of questions we expect it to answer are ones that do not refer

to the microscopic details of the lattice model. For example, from the effective field theory we will calculate the asymptotics of the probability that two points lie on the same loop, when the separation between the points is large compared to the lattice spacing. From this and related quantities the conformational exponents of compact polymers can be extracted.

The field theory of the FPL² model is defined by the Euclidean action for the coarse grained height \mathbf{h} . Consider a typical configuration of the oriented FPL² model which is equivalent to the colouring model. It consists of domains of ideal states. To each ideal state domain we assign a coarse grained height, defined earlier as the average microscopic height over the domain. In the continuum limit we assume that this height is a smoothly varying function of the basal plane coordinates (x^1, x^2) . The partition function that takes into account only the large scale fluctuations of the height can be written as a functional integral,

$$Z_{>} = \int \mathcal{D}\mathbf{h} \exp(-S[\mathbf{h}]), \quad (5.1)$$

where S is the Euclidean action of a Liouville field theory with imaginary couplings [7]. The Liouville action contains three terms,

$$S = S_E + S_B + S_L. \quad (5.2)$$

Each one has a concrete geometrical interpretation in the FPL² model, which we describe next.

A. Elastic term

The first term in the effective action for the FPL² model describes the elastic fluctuations of the interface. It gives less weight to configurations that deviate from the flat states, by penalising finite gradients of the height. This term is entropic in origin. Namely, in order to change the colour of a particular bond in the four-colouring representation of the loop model, say $\mathbf{C} \rightarrow \mathbf{B}$, all the \mathbf{C} 's and \mathbf{B} 's have to be interchanged along the \mathbf{CB} loop which contains the chosen bond. This transformation we call a *loop flip*; see Fig. 6. The ideal states *maximise* the number of loops of alternating colour and consequently they have the largest entropy of loop flips.

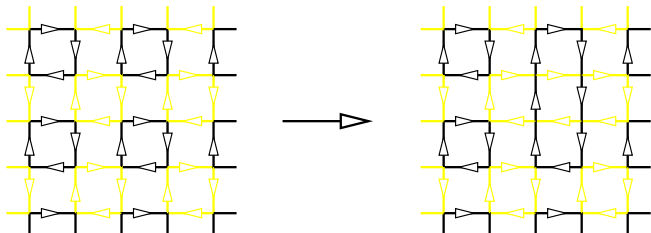


FIG. 6. A loop flip changes one oriented loop configuration into another. Here the bond states \mathbf{C} and \mathbf{B} are exchanged along a single \mathbf{BC} plaquette (cfr. Fig. 4c).

In its most general form the elastic term in the effective action can be written as a gradient expansion,

$$S_E = \frac{1}{2} \int d^2\mathbf{x} K_{\alpha\beta}^{ij} \partial_i h^\alpha \partial_j h^\beta, \quad (5.3)$$

where higher powers of the height gradients and higher derivatives of the height are less relevant at large scales. The stiffness tensor $K_{\alpha\beta}^{ij}$ nominally has 36 components; the indices $i, j = 1, 2$ are for the basal plane coordinates, whilst $\alpha, \beta = 1, 2, 3$ label the three components of the height. Summation over repeated indices is assumed throughout.

The number of independent non-zero components of the stiffness tensor (i.e., elastic constants) is actually only *three*, once all the symmetries of the FPL² model are taken into account. The relevant symmetry transformations, that is the ones that become the symmetries of the effective action, are the ones that leave the weights of oriented loop configurations unchanged. First, there are the lattice symmetries, translations and rotations, which cut the number of independent elastic constants down to six. The terms that are allowed in S_E are scalars under rotations in the basal plane $\{(x^1, x^2)\}$, and they are necessarily of the form $\partial h^\alpha \cdot \partial h^\beta$, where $\partial = (\partial_1, \partial_2)$ is the usual gradient. Second, the FPL² model possesses colour symmetries,

$$\mathbf{A} \leftrightarrow \mathbf{B} : e_b \leftrightarrow -e_b \text{ and } z_1 \leftrightarrow z_3 \quad (5.4)$$

and

$$\mathbf{C} \leftrightarrow \mathbf{D} : e_g \leftrightarrow -e_g \text{ and } z_1 \leftrightarrow -z_3, \quad (5.5)$$

which interchange the colours and at the same time transform the microscopic heights. Taking into account the colour symmetries the elastic contribution to the action takes on the form:

$$S_E = \frac{1}{2} \int d^2\mathbf{x} \{ K_{11} [(\partial h^1)^2 + (\partial h^3)^2] + 2K_{13} (\partial h^1 \cdot \partial h^3) + K_{22} (\partial h^2)^2 \}. \quad (5.6)$$

Furthermore, by introducing a change of coordinates in height space,

$$H^1 = \frac{1}{2}(h^1 - h^3), \quad H^2 = h^2, \quad H^3 = \frac{1}{2}(h^1 + h^3) \quad (5.7)$$

S_E becomes diagonal,

$$S_E = \frac{1}{2} \int d^2\mathbf{x} g_\alpha (\partial H^\alpha)^2. \quad (5.8)$$

The three coupling constants g_α ($\alpha = 1, 2, 3$) are linearly related to the three elastic constants,

$$g_1 = 2(K_{11} - K_{13}), \quad g_2 = K_{22}, \quad g_3 = 2(K_{11} + K_{13}). \quad (5.9)$$

The appearance of *three* elastic constants is rather intriguing from the viewpoint of loop models that have been solved previously. The Q -state Potts, the $O(n)$, and the honeycomb FPL models are all characterised by a *single* coupling constant, which has been determined case by case from their exact solutions. Below we will show that all three couplings in Eq. (5.8) can be calculated exactly from the *loop ansatz* introduced in Ref. [7].³ The ansatz states that the operator which enforces the complex weights assigned to oriented loops is *marginal* in the renormalisation group sense. This property of the field theory is intimately related to the random geometry of loops; we elaborate on this important point in Section V C 2.

B. Boundary term

The mapping of the loop model to an oriented loop model with local complex weights $\lambda(\mathbf{x})$ (Eq. (4.3)) fails for loops that experience the boundary. For example, if we define the FPL² model on a cylinder then loops that wind around the cylinder will not be weighted properly. The winding loop has an equal number of left and right turns and hence it will be assigned a weight one. Summing over the two orientations gives a weight two, and not the correct n_b or n_g , depending on the flavour. To correctly weight these loops one introduces a boundary term into the effective action,

$$S_B = \frac{i}{4\pi} \int d^2\mathbf{x} (\mathbf{e}_0 \cdot \mathbf{h}) \mathcal{R}; \quad (5.10)$$

\mathcal{R} is the scalar curvature and \mathbf{e}_0 is the *background* electric charge, which is to be determined. Since we are only concerned with the situation where the lattice on which the FPL² model is defined is flat, the scalar curvature vanishes everywhere except at the boundary.

To determine \mathbf{e}_0 we consider the FPL² model on the cylinder. The scalar curvature of the cylinder is proportional to the difference of two delta functions situated at the two far ends of the cylinder: $\mathcal{R} = 4\pi[\delta(+\infty) - \delta(-\infty)]$. Therefore S_B has the effect of placing vertex operators $\exp(\pm i\mathbf{e}_0 \cdot \mathbf{h})$ at $x^2 = \pm\infty$; here x^2 is the coordinate along the length of the cylinder. These vertex operators assign an additional weight $\exp(i\mathbf{e}_0 \cdot (\mathbf{h}(+\infty) - \mathbf{h}(-\infty)))$ to oriented loop configurations on the cylinder. Now, in order for $\mathbf{h}(+\infty) - \mathbf{h}(-\infty)$

to be non-zero there must be at least a single winding loop present. If this winding loop is black, then the height difference is \mathbf{A} or \mathbf{B} depending on its orientation; similarly if the loop is grey the height difference is \mathbf{C} or \mathbf{D} . Furthermore if the background charge is chosen so as to satisfy

$$\begin{aligned} \mathbf{e}_0 \cdot \mathbf{A} &= \pi e_b & \mathbf{e}_0 \cdot \mathbf{B} &= -\pi e_b \\ \mathbf{e}_0 \cdot \mathbf{C} &= \pi e_g & \mathbf{e}_0 \cdot \mathbf{D} &= -\pi e_g \end{aligned} \quad (5.11)$$

then the winding loops will be assigned their proper weights. This is again seen by summing over the two possible orientations of the winding loop. In the normalisation chosen for the colour vectors, Eq. (4.2), the unique solution of the system of linear equations in Eq. (5.11) is

$$\mathbf{e}_0 = -\frac{\pi}{2}(e_g + e_b, 0, e_g - e_b). \quad (5.12)$$

This calculation of the *vector* background charge generalises the scalar case studied previously [6].

C. Liouville potential

The elastic term and the boundary term make up the usual Coulomb gas approach to two-dimensional critical phenomena. Recently we have argued that this description is incomplete and that an extra term S_L must be added to the effective action. To see this consider a large loop in the bulk, one that does not experience the boundary. Without the extra term this loop would be weighted exclusively by the bulk term S_E . There are two problems with this: S_E is real whilst an oriented loop should be weighted by a complex phase, and, S_E does not distinguish between the two orientations of a loop which are assigned different weights. We conclude that an extra *bulk* term is necessary!

The most general form of a bulk term is

$$S_L = \int d^2\mathbf{x} w[\mathbf{h}(\mathbf{x})], \quad (5.13)$$

where $\exp(-w[\mathbf{h}(\mathbf{x})])$ is the scaling limit of $\lambda(\mathbf{x})$ in Eq. (4.3). In this sense S_L is energetic in origin, as opposed to S_E , which we argued in Sec. V A accounts for the entropy of edge colourings.

Microscopically, the vertex weight λ can be written in terms of the colours of the bonds around the particular vertex as $\lambda = \exp(-w)$ where

³The coupling constant g for all the loop models known to date can be calculated using this method, therefore dispensing with the need for an exact solution.

$$\begin{aligned}
w(\mathbf{B}, \mathbf{C}, \mathbf{A}, \mathbf{D}) &= 0, \\
w(\mathbf{B}, \mathbf{D}, \mathbf{A}, \mathbf{C}) &= 0, \\
w(\mathbf{A}, \mathbf{B}, \mathbf{C}, \mathbf{D}) &= \mp i \frac{\pi}{4} (e_g + e_b), \\
w(\mathbf{B}, \mathbf{A}, \mathbf{C}, \mathbf{D}) &= \mp i \frac{\pi}{4} (e_g - e_b), \\
w(\mathbf{A}, \mathbf{B}, \mathbf{D}, \mathbf{C}) &= \mp i \frac{\pi}{4} (e_b - e_g), \\
w(\mathbf{B}, \mathbf{A}, \mathbf{D}, \mathbf{C}) &= \mp i \frac{\pi}{4} (-e_b - e_g); \quad (5.14)
\end{aligned}$$

the top sign is for even vertices whilst the bottom sign applies to odd vertices of the square lattice. Here we adopt the notation $(\sigma_1, \sigma_2, \sigma_3, \sigma_4)$ for the ordering of the colours around a vertex by listing the colours clockwise from the leftmost bond. The operator w is completely specified by the values it takes on the six edge colourings listed above since it does not change under cyclic permutations of its arguments.

By explicitly going through the six colour configurations listed above it is easily checked that

$$w(\mathbf{x}) = \frac{i}{16} \mathbf{e}_0 \cdot \mathbf{Q}(\mathbf{x}), \quad (5.15)$$

where the cross-staggered operator [28] is defined by

$$\mathbf{Q}(\mathbf{x}) = \pm [\sigma_1(\mathbf{x}) - \sigma_3(\mathbf{x})] \times [\sigma_2(\mathbf{x}) - \sigma_4(\mathbf{x})]. \quad (5.16)$$

Since $\mathbf{Q}(\mathbf{x})$ is manifestly invariant under 90° rotations of the colours around \mathbf{x} , Eq. (5.15) is seen to hold true for any distribution of the colours around a given vertex.

In order to find the coarse grained version of $w(\mathbf{x})$ we express it as a function of the height field $\mathbf{h}(\mathbf{x})$. First note that the microscopic operator $w(\mathbf{x})$ is *uniform* in each of the ideal states of the four colouring model. As such it defines a function on the ideal state graph $w(\mathbf{h})$, where $\mathbf{h} \in \mathcal{I}$ is the coarse grained height. Furthermore, it is a periodic function of \mathbf{h} and it can therefore be written as a Fourier sum:

$$w(\mathbf{h}) = \sum_{\mathbf{e} \in \mathcal{R}_w^*} \tilde{w}_{\mathbf{e}} \exp(i\mathbf{e} \cdot \mathbf{h}). \quad (5.17)$$

The electric charges appearing in the sum take their values in the sub-lattice $\mathcal{R}_w^* \subset \mathcal{R}^*$, which is the lattice reciprocal to the lattice of *periods* of $w(\mathbf{h})$. In the continuum limit the coarse-grained height \mathbf{h} is promoted into the height field $\mathbf{h}(\mathbf{x})$, and the scaling limit of the operator w is obtained by replacing \mathbf{h} by $\mathbf{h}(\mathbf{x})$ in Eq. (5.17). Therefore $w[\mathbf{h}(\mathbf{x})]$ is a sum of vertex operators,

$$w[\mathbf{h}(\mathbf{x})] = \sum_{\mathbf{e} \in \mathcal{R}_w^*} \tilde{w}_{\mathbf{e}} \exp(i\mathbf{e} \cdot \mathbf{h}(\mathbf{x})), \quad (5.18)$$

of which only the most relevant one(s) are kept in the effective action. Since the relevance of an operator is determined by its scaling dimension we turn to this calculation next.

1. Dimensions of charge operators

In the Coulomb gas formalism operators are associated with either electric or magnetic charges. Electric operators are vertex operators $\exp(i\mathbf{e} \cdot \mathbf{h})$ and they appear as the scaling limits of microscopic operators in the FPL² model that can be expressed as local functions of the colours; the loop-weight operator is one example.

Magnetic operators on the other hand cannot be expressed as local functions of the height but can be thought of as a constraint on the height field that generates a topological defect of strength \mathbf{m} . If \mathbf{x} is the position of the defect core then the net height increase around any loop that encloses \mathbf{x} is \mathbf{m} (assuming no other defects are encircled). Geometrical exponents for loops in the FPL² model are given by dimensions of electric and magnetic operators in the associated Coulomb gas.

For an operator that has total electromagnetic charge (\mathbf{e}, \mathbf{m}) , where $\mathbf{e} = (e_1, e_2, e_3)$ and $\mathbf{m} = (m^1, m^2, m^3)$, the scaling dimension is the sum of the electric and magnetic dimensions,⁴

$$2x(\mathbf{e}, \mathbf{m}) = \frac{1}{2\pi} \left[\frac{1}{g_\alpha} E_\alpha (E_\alpha - 2E_{0\alpha}) + g_\alpha (M^\alpha)^2 \right], \quad (5.19)$$

where

$$E_1 = e_1 - e_3, \quad E_2 = e_2, \quad E_3 = e_1 + e_3 \quad (5.20)$$

and

$$M^1 = \frac{1}{2}(m^1 - m^3), \quad M^2 = m^2, \quad M^3 = \frac{1}{2}(m^1 + m^3) \quad (5.21)$$

are the electric and magnetic charge vectors in the basis in which the elastic term in the action is diagonal. Since the magnetic charges are given by height differences they must transform according to Eq. (5.7), whilst the electric charges transform in a dual fashion (cfr. their appearance in the vertex operators).

⁴The derivation of Eq. (5.19) is an exercise in Gaussian integration and is reviewed in Appendix A.

2. Loop ansatz

With the dimension formula in hand, we can settle the issue of the most relevant operators appearing in the Fourier expansion of $w(\mathbf{h})$; see Eq. (5.18). There are twelve vertex operators to choose from corresponding to the twelve (110)-type vectors in the bcc lattice \mathcal{R}^* ; these are the shortest vectors in the lattice \mathcal{R}_w^* . To find which of these electric charges minimise $x(\mathbf{e}, 0)$ (Eq. (5.19)) it is convenient to first consider the simpler case of the FPL² model for $n_b = n_g$.

For the FPL² model with equal fugacities for the black and grey loops the effective action is considerably simplified. Namely, in this case the cyclic permutation of the colours,

$$\begin{aligned} (\mathbf{A}, \mathbf{B}, \mathbf{C}, \mathbf{D}) &\leftrightarrow (\mathbf{B}, \mathbf{C}, \mathbf{D}, \mathbf{A}) : \\ (z_1, z_2, z_3) &\leftrightarrow (-z_1, z_3, -z_2) \end{aligned} \quad (5.22)$$

does not change the vertex weight λ , and is thus an additional symmetry of the action S . This symmetry implies that $K_{13} = 0$ and $K_{22} = K_{11}$ in Eq. (5.6). Consequently there is only one elastic constant, $K \equiv K_{11}$. This then simplifies the formula for the dimension of an electromagnetic charge,

$$2x(\mathbf{e}, \mathbf{m}) = \frac{1}{2\pi K} \mathbf{e} \cdot (\mathbf{e} - 2\mathbf{e}_0) + \frac{K}{2\pi} \mathbf{m}^2, \quad (5.23)$$

where from Eq. (5.12) it follows that the background charge in this case has only one non-zero component, $\mathbf{e}_0 = -\pi(e_b, 0, 0)$. Now it is a simple matter to check that of the twelve (110)-type vectors in the lattice of electric charges \mathcal{R}^* , the four charges

$$\begin{aligned} \mathbf{e}^{(1)} &= (-\pi, 0, +\pi), \\ \mathbf{e}^{(2)} &= (-\pi, 0, -\pi), \\ \mathbf{e}^{(3)} &= (-\pi, +\pi, 0), \\ \mathbf{e}^{(4)} &= (-\pi, -\pi, 0) \end{aligned} \quad (5.24)$$

are degenerate in dimension and they minimise $2x(\mathbf{e}, 0)$. These are therefore the electric charges of the vertex operators that are kept in the action.

Now we turn to the *loop ansatz* which states that the operator $w(\mathbf{h})$ is exactly marginal in the renormalisation group sense. This is the statement that the loop weight does not renormalise at large scales. The geometrical meaning of this becomes obvious when one realises that the number of loops inside a domain of size ρ , whose linear size is *comparable* to ρ , is thermodynamically conjugate to the loop weight at scale ρ . Thus the loop ansatz states that the number of large loops does not grow with scale (more precisely it is sufficient to assume that it does not grow faster than any power of the scale). The analogous statement can be proven rigorously for critical percolation where it is the source of hyperscaling [35].

The assumption that there is of order one loop at every scale is linked to the variance of the height difference between two points in the basal plane, separated by a macroscopic distance $|\mathbf{x}|$. Namely, if we assume that when going from one point to the other there is of order one contour loop that is crossed at every *scale*, and further assuming that the directions of these contours are independent from scale to scale, it follows from the law of large numbers that the variance of the height difference grows as the number of contours crossed, that is as $\log(|\mathbf{x}|)$. This of course is nothing but the large $|\mathbf{x}|$ behaviour of $\langle (H^\alpha(\mathbf{x}) - H^\alpha(0))^2 \rangle$ calculated in the Gaussian model of Eq. (5.8).

The loop ansatz, or in other words the marginality hypothesis for the loop weight operator, simply translates into a statement about its scaling dimension:

$$x(\mathbf{e}^{(i)}, 0) = 2 \quad i = 1, 2, 3, 4. \quad (5.25)$$

This, using the dimension formula Eq. (5.23), leads to a formula for the single elastic constant K .

In the general case $n_b \neq n_g$, the scaling dimensions of the four electric charges identified above are

$$\begin{aligned} x(\mathbf{e}^{(1)}, 0) &= \pi \frac{1 - e_b}{g_1}, \\ x(\mathbf{e}^{(2)}, 0) &= \pi \frac{1 - e_g}{g_3}, \\ x(\mathbf{e}^{(3)}, 0) &= x(\mathbf{e}^{(4)}, 0) = \frac{\pi}{4} \left(\frac{1 - 2e_b}{g_1} + \frac{1}{g_2} + \frac{1 - 2e_g}{g_3} \right); \end{aligned} \quad (5.26)$$

the last two remain degenerate in dimension. The dimensions of the first two charges are also equal due to the ‘‘duality’’ transformation of the FPL² model which exchanges the two flavours, $n_b \leftrightarrow n_g$. This transforms the microscopic heights $z_2 \rightarrow -z_2$ and $z_3 \rightarrow -z_3$ (and similarly for the appropriate components of the height field). Furthermore, the elastic constants K_{11} and K_{22} in Eq. (5.6) are unchanged, whilst $K_{13} \rightarrow -K_{13}$. Finally, from Eq. (5.9) it follows that the duality transformation exchanges the couplings $g_1 \leftrightarrow g_3$ thus rendering $\mathbf{e}^{(1)}$ and $\mathbf{e}^{(2)}$ degenerate in dimension, as the FPL² model is self-dual.

Unlike the case of $n_b = n_g$, the loop ansatz in the general case requires that at least *two* of the electric charges $\mathbf{e}^{(i)}$ ($i = 1, 2, 3, 4$) remain marginal, thus enforcing the non-renormalisability of the two fugacities n_b and n_g . If we now further *assume* that these charges are unrelated by the ‘‘duality’’ transformation described above, it follows that in fact all four are marginal. The three couplings are then simply calculated by setting the right hand sides of Eq. (5.26) equal to 2. We find:

$$\begin{aligned} g_1 &= \frac{\pi}{2}(1 - e_b), \\ g_3 &= \frac{\pi}{2}(1 - e_g), \\ \frac{1}{g_2} &= \frac{1}{g_1} + \frac{1}{g_3}. \end{aligned} \quad (5.27)$$

One final comment is in order. The relation $1/g_2 = 1/g_1 + 1/g_3$ comes as somewhat of a surprise, as it was not anticipated on symmetry grounds. Of course, since a particular point in the critical region of the FPL² model is determined by two parameters, n_b and n_g , one relation between the three couplings is to be expected. It is therefore an interesting open question whether a critical loop model can be constructed in which g_2 would be unconstrained.⁵

With the values of the couplings g_1, g_2 , and g_3 in hand, as well as the formula for the scaling dimensions of charged operators, Eq. (5.19), we are fully equipped to calculate critical exponents of the FPL² model. In particular, in the next section we calculate the formulae for the central charge and the geometrical exponents associated with loops as a function of the loop fugacities, n_b and n_g , for the whole critical region of the model.

VI. CENTRAL CHARGE

We now turn to the calculation of the central charge in the critical region, $0 \leq n_b, n_g \leq 2$. Exactly at the point $(n_b, n_g) = (2, 2)$ the background charge vanishes, $\mathbf{e}_0 = \mathbf{0}$, and the action consists only of the elastic term S_E given by Eq. (5.8). Since this is then simply a theory of three free massless bosonic fields we conclude that, in this case, $c = 3$ [28].

For a general value of the background charge this generalises to [36]

$$c = 3 + 12x(\mathbf{e}_0, 0) . \quad (6.1)$$

One way to rationalise the factor of 12 is to compare the coefficients of the finite-size corrections in the well-known formulae [37,38]

$$f_0(\infty) - f_0(L) = \frac{\pi c}{6L^2} + \dots \quad (6.2)$$

$$f_i(L) - f_0(L) = \frac{2\pi x_i}{L^2} + \dots , \quad (6.3)$$

where $f_{0,i}(L)$ is the free energy density on a cylinder of circumference L , the subscript 0 referring to the vacuum and i to the case when an operator of scaling dimension x_i is inserted. The physical meaning of Eq. (6.1) is that the presence of the background charge $-\mathbf{e}_0$ and $+\mathbf{e}_0$ at the two ends of the cylinder – lowers the free energy and with it the central charge.

Now using the dimension formula, Eq. (5.19), and inserting the values of the couplings g_α from Eq. (5.27), we arrive at

$$c = 3 - 6 \left(\frac{e_b^2}{1 - e_b} + \frac{e_g^2}{1 - e_g} \right), \quad (6.4)$$

where we recall that $n_b = 2 \cos(\pi e_b)$ and similarly for n_g . In Table I the numerically calculated values of the conformal charge are compared to the above formula, and excellent agreement is found.

VII. GEOMETRICAL SCALING DIMENSIONS

A. Two-string dimension

In addition to the central charge, the Coulomb gas representation of the loop model provided by the Liouville field theory, Eq. (5.2), allows for the evaluation of various geometrical scaling dimensions. As an example of such a quantity, consider the probability $G_2(r)$ that two points separated by a distance r lie on the same, say, black loop. In the critical phase we expect this probability to decay as $G_2(r) \sim r^{-2x_2}$, which defines the scaling dimension x_2 . Since a black loop is represented as a sequence of alternating **A** and **B**-coloured edges it follows from the colouring constraint that the microscopic heights \mathbf{z} just outside this loop differ by integer multiples of **C** and **D** only. In other words, a black loop is a *contour* loop for the component of the height along the direction perpendicular to both **C** and **D**, i.e., the $(1, 0, -1)$ direction in height space. Similarly the grey loops are contour loops for the height component along the $(1, 0, 1)$ direction.

It has been argued that the scaling dimension governing the probability that two points belong to the same contour loop of a random Gaussian surface equals 1/2, independent of the stiffness [39]. Thus, for $(n_b, n_g) = (2, 2)$ when $\mathbf{e}_0 = \mathbf{0}$ and the effective field theory is Gaussian, we expect $x_2 = 1/2$. For other values of the fugacities the Gaussian theory is modified by the background charge and the same argument cannot be made.

⁵This possibility was suggested to us by D. Huse.

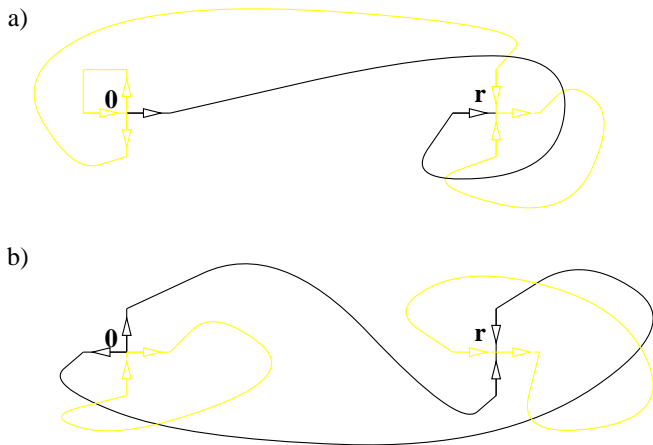


FIG. 7. Defect configurations used to calculate geometrical exponents x_1 (a) and x_2 (b) in the FPL² model. In (a) there is a single oriented black loop segment and a single oriented grey loop segment propagating from $\mathbf{0}$ to \mathbf{r} , whilst in (b) there are two oriented black loop segments between $\mathbf{0}$ and \mathbf{r} .

A more illuminating way of making contact with the interface representation is to view $G_2(r)$ as a two-string correlation function associated with defect configurations where two black strings emanating from the origin annihilate one another at a distant point \mathbf{r} ; see Fig. 7b. This can be accomplished by rewriting $G_2(r)$ as $Z(r)/Z$, where Z is the partition function defined by Eq. (4.3), and $Z(r)$ is similarly defined but with the summation restricted to those configurations \mathcal{G}'_r where an oriented black loop passes through the points $\mathbf{0}$ and \mathbf{r} . Now consider reversing the direction of one half of the loop, so that instead of having one oriented loop passing through $\mathbf{0}$ and \mathbf{r} we have two oriented loop segments directed from $\mathbf{0}$ to \mathbf{r} [6]. This corresponds to the introduction of defect configurations at these two points, where we have violated the edge-colouring constraint. At $\mathbf{0}$ we find a $(\mathbf{C}, \mathbf{D}, \mathbf{A}, \mathbf{A})$ configuration of colours which in the height language corresponds to a vortex of strength

$$\mathbf{m}_2 = \mathbf{A} - \mathbf{B} = (-2, 0, 2). \quad (7.1)$$

The strength of the vortex (its Burgers charge) at $\mathbf{0}$ is calculated as the total height change around $\mathbf{0}$. Similarly, at \mathbf{r} we have the corresponding antivortex $(\mathbf{B}, \mathbf{B}, \mathbf{C}, \mathbf{D})$ of strength $-\mathbf{m}_2$ as illustrated in Fig. 7b.

In order to calculate x_2 for general values of the loop fugacities we have to take into account the effect of the complex phase factors associated with oriented loops. Namely, when one or more, say, black strings are associated with a vortex-antivortex configuration, spurious phase factors $\exp(\pm i\pi e_b)$ will arise whenever a black loop segment winds around one of the vortex cores [6]; for example, in Fig. 7b one of the two black strings winds once around point \mathbf{r} . The spurious winding phase can be removed by inserting the vertex operator $\exp(i\mathbf{e}_b \cdot \mathbf{h})$ at the positions of both vortex cores. Since a black loop has

alternating \mathbf{A} and \mathbf{B} colours the electric charge \mathbf{e}_b must satisfy

$$\begin{aligned} \mathbf{e}_b \cdot \mathbf{A} &= \pi e_b, & \mathbf{e}_b \cdot \mathbf{B} &= -\pi e_b, \\ \mathbf{e}_b \cdot \mathbf{C} &= 0, & \mathbf{e}_b \cdot \mathbf{D} &= 0. \end{aligned} \quad (7.2)$$

Similarly, if there are grey strings propagating between two vertices the spurious phase factors associated with winding configurations are corrected with vertex operators whose electric charge \mathbf{e}_g is determined by

$$\begin{aligned} \mathbf{e}_g \cdot \mathbf{A} &= 0, & \mathbf{e}_g \cdot \mathbf{B} &= 0, \\ \mathbf{e}_g \cdot \mathbf{C} &= \pi e_g, & \mathbf{e}_g \cdot \mathbf{D} &= -\pi e_g. \end{aligned} \quad (7.3)$$

Using Eq. (4.2) for the colour-vectors we find,

$$\mathbf{e}_b = -\frac{\pi}{2}(e_b, 0, -e_b), \quad \mathbf{e}_g = -\frac{\pi}{2}(e_g, 0, e_g). \quad (7.4)$$

Going back to the two-string operator we conclude that it has total electromagnetic charge $(\mathbf{e}_b, \mathbf{m}_2)$.

Finally, from the general expression for the scaling dimension of an electro-magnetic operator, Eq. (5.19), it follows that

$$2x_2 = 2x(\mathbf{e}_b, \mathbf{m}_2) = (1 - e_b) - \frac{e_b^2}{1 - e_b}. \quad (7.5)$$

In Table V exact values of x_2 calculated from this formula are compared to numerical results, and excellent agreement is found.

Interestingly the expression for x_2 is *independent* of e_g , i.e., it is not affected by the fugacity of grey loops. This observation conforms to our understanding of the scaling of compact polymers. The compact polymer problem is recovered in the limit $n_b \rightarrow 0$ in which case there is a single black loop on the lattice. Since the loop fills space its Hausdorff dimension is necessarily $D = 2$. Scaling tells us that [40]

$$D = 2 - x_2 \quad (7.6)$$

from which the result $x_2 = 0$ follows, *independent* of the fugacity of grey loops. The fact that our formula reproduces this simple result in the $n_b = 0$ ($e_b = 1/2$) case provides a non-trivial check on its validity.

B. One-string dimension

The scaling dimension x_1 corresponding to one black and one grey string propagating between two points on the lattice, can be computed in a way that is completely analogous to the case of two black strings discussed above. (Note that the fully packing constraint ensures that if there is a single black string between two points then these points are also connected by a grey string; see Fig. 7a.) Choosing one point on the even sub-lattice and the other on the odd, leads to the appearance

of the defect configuration $(\mathbf{A}, \mathbf{C}, \mathbf{C}, \mathbf{D})$ on both sites of the square lattice. These in turn correspond to vortices in the height representation with topological charges $\pm \mathbf{m}_1$, where

$$\mathbf{m}_1 = \mathbf{C} - \mathbf{B} = (-2, -2, 0). \quad (7.7)$$

Since strings of both flavours are now present the compensating electric charge is $\mathbf{e}_b + \mathbf{e}_g = \mathbf{e}_0$. Hence

$$\begin{aligned} 2x_1 &= 2x(\mathbf{e}_0, \mathbf{m}_1) \\ &= \frac{1}{4} [(1 - e_b) + (1 - e_g)] \\ &\quad + \frac{(1 - e_b)(1 - e_g)}{(1 - e_b) + (1 - e_g)} - \left[\frac{e_b^2}{1 - e_b} + \frac{e_g^2}{1 - e_g} \right]. \end{aligned} \quad (7.8)$$

There are of course several different ways of choosing the defect configurations (in this case, eight), but it should hardly come as a surprise that they all lead to the same expression for the scaling dimension.

Unlike x_2 , x_1 depends on both loop fugacities. Going back to our original motivation, the compact polymer problem ($n_b = 0 \Rightarrow e_b = 1/2$), x_1 determines the value of the conformational exponent $\gamma = 1 - x_1$, which describes the scaling of the number of compact polymers with the number of monomers. We see that depending on e_g there will be a continuum of γ 's. How do we interpret this?

First note that the problem of counting the number of conformations of a single compact polymer is the case $n_g = 1$ ($e_g = 1/3$) which simply assigns equal weights to all conformations. Using Eq. (7.8) this choice leads to $x_1 = -5/112$ and to the result $\gamma = 117/112$ advertised in the abstract. Changing n_g (e_g) away from $n_g = 1$, on the other hand, has the effect of favouring certain compact polymer conformations over others depending on the number of loops formed by the uncovered (grey) bonds. In this sense the weight assigned to grey loops can be thought of as an interaction between the monomers of the compact polymer, albeit a peculiar non-local one. Nonetheless, it is interesting that this interaction changes the scaling properties of the compact polymer leading to a continuously varying exponent γ (more on this in the Discussion).

C. Many-string dimensions

The dimensions x_1 and x_2 given above are contained in a more general set of string dimensions x_{s_b, s_g} governing the probability of having s_b black loop segments and s_g grey loop segments propagating between two points on the lattice [18]. More precisely, we consider two microscopic regions centred around points separated by a macroscopic distance, one region being the source and the other the sink of the oriented loop segments. Since

the defect configurations obtained by violations of the edge colouring constraint must necessarily give rise to an *even* number of strings we will only consider the case when $s_b + s_g$ is even.

Consider first the case $s_b = 2k_b$ and $s_g = 2k_g$. The appropriate magnetic charge is obtained by combining k_b vortices with charge $\mathbf{A} - \mathbf{B} = (-2, 0, 2)$, and k_g vortices with charge $\mathbf{C} - \mathbf{D} = (-2, 0, -2)$. The defect with charge $\mathbf{A} - \mathbf{B}$ acts as a source of two black segments, whilst $\mathbf{C} - \mathbf{D}$ is associated with two grey loop segments. We also need to introduce the electric charge $e_b + e_g$ to compensate for the extra winding phase associated with the black and grey loop segments. The total electromagnetic charge is therefore

$$\begin{aligned} [\mathbf{e}_{2k_b, 2k_g}, \mathbf{m}_{2k_b, 2k_g}] &= \\ [\mathbf{e}_b(1 - \delta_{k_b, 0}) + \mathbf{e}_g(1 - \delta_{k_g, 0}), -2(k_b + k_g, 0, k_g - k_b)], \end{aligned} \quad (7.9)$$

and from the dimension formula, Eq. (5.19), we find

$$\begin{aligned} 2x_{2k_b, 2k_g} &= \\ (1 - e_b)k_b^2 + (1 - e_g)k_g^2 + \\ - \frac{e_b^2}{1 - e_b}(1 - \delta_{k_b, 0}) - \frac{e_g^2}{1 - e_g}(1 - \delta_{k_g, 0}). \end{aligned} \quad (7.10)$$

This formula generalises Eq. (7.5).

Similarly, for $s_b = 2k_b - 1$ and $s_g = 2k_g - 1$ the electromagnetic charge is

$$\begin{aligned} [\mathbf{e}_{2k_b - 1, 2k_g - 1}, \mathbf{m}_{2k_b - 1, 2k_g - 1}] &= \\ [\mathbf{e}_0, -2(k_b + k_g - 1, 1, k_g - k_b)]; \end{aligned} \quad (7.11)$$

the magnetic charge is obtained by combining $k_b - 1$ defects of charge $\mathbf{A} - \mathbf{B}$, $k_g - 1$ defects of charge $\mathbf{C} - \mathbf{D}$, and a single defect of charge $\mathbf{C} - \mathbf{B}$ which produces the remaining single black and grey strings originating from the same vertex. The scaling dimension is found to be

$$\begin{aligned} 2x_{2k_b - 1, 2k_g - 1} &= \\ \frac{1}{4} [(1 - e_b)(2k_b - 1)^2 + (1 - e_g)(2k_g - 1)^2] + \\ \frac{(1 - e_b)(1 - e_g)}{(1 - e_b) + (1 - e_g)} - \left[\frac{e_b^2}{1 - e_b} + \frac{e_g^2}{1 - e_g} \right]. \end{aligned} \quad (7.12)$$

This generalises the expression given in Ref. [7] and correctly reduces to Eq. (7.8) for $k_b, k_g = 1$.

D. Thermal dimension

We now turn our attention to the thermal scaling dimension. The FPL² model can be thought of as the zero-temperature limit of a more general model where we allow for thermal excitations that violate the close packing constraint. In this sense the temperature variable is thermodynamically conjugate to the constraint that

every vertex be visited by (say) a black loop. An appropriate defect configuration for computing x_T within the FPL² model is therefore $(\mathbf{C}, \mathbf{D}, \mathbf{C}, \mathbf{D})$. This is a vortex of strength

$$\mathbf{m}_T = 2(\mathbf{C} + \mathbf{D}) = (0, -4, 0), \quad (7.13)$$

and since no strings terminating in the bulk are generated there is no compensating electric charge. The scaling dimension is then

$$2x_T = 2x(0, \mathbf{m}_T) = 4 \frac{(1 - e_b)(1 - e_g)}{(1 - e_b) + (1 - e_g)}. \quad (7.14)$$

The exact values of x_T quoted in Table II are calculated using this formula. The numerical results are in excellent agreement.

E. Boundary-string dimensions

The simplest example of a string operator that cannot be accessed within the formalism presented above is that of one black and no grey strings propagating between two vertices of the square lattice. Since this configuration has an odd number of strings connecting two sites of the lattice these two sites necessarily reside on the *boundary*.

If we define the FPL² model on the cylinder, as will be the case when we construct its transfer matrix in Sec. IX, a single black string can be enforced to run along the length of the cylinder if its circumference is chosen *odd*. Taking our cue from the formulae derived above for the bulk string operators we *guess* the formula

$$X = \frac{1}{8} + \frac{1 - e_b}{8} - \frac{1}{2} \frac{e_b^2}{1 - e_b} \quad (7.15)$$

from the numerical results shown in Table III. X is the scaling dimension of the boundary operator which corresponds to a single black (or grey) string.

The Coulomb gas interpretation of the second and third term in Eq. (7.15) is rather apparent when one compares them to Eq. (7.5). The second term can be rationalised as coming from a magnetic charge $(-1, 0, 1)$ which is half the charge \mathbf{m}_2 in Eq. (7.1), associated with two black strings; this is saying that we have a partial dislocation generated at the boundary. The third term is due to the compensating electric charge e_b for a single black string, same as in the two-string case.

The first, constant term does not have an immediate interpretation. A possible scenario is that it is due to the boundary condition imposed on the height by virtue of having a cylinder of odd circumference. Namely, a translation along the periodic coordinate by an amount equal to the circumference (L) exchanges an even site for an odd site (and *vice versa*) resulting in a transformation of the height: $\mathbf{h}(x^1, x^2) = \mathbf{P}\mathbf{h}(x^1 + L, x^2)$. Since $\mathbf{P}^2 = 1$ this boundary condition can be thought of as an insertion of

a twist operator into the partition function. The twist operator has dimension $1/8$ regardless of the stiffness of the interface [41].

The above considerations permit us to calculate the scaling dimension for the general case of an odd number of strings. For definiteness we consider the case of $s_b = 2k_b - 1$ and $s_g = 2k_g$. The magnetic charge pertaining to this situation is found by combining $2k_b - 1$ defects of charge $\frac{1}{2}(\mathbf{A} - \mathbf{B})$ with k_g defects of charge $\mathbf{C} - \mathbf{D}$, totaling

$$[\mathbf{e}_{2k_b-1, 2k_g}, \mathbf{m}_{2k_b-1, 2k_g}] = \quad (7.16)$$

$$[\mathbf{e}_b + \mathbf{e}_g(1 - \delta_{k_g, 0}), (1 - 2k_b - 2k_g, 0, 2k_b - 2k_g - 1)].$$

Taking into account the contribution from the twist operator, i.e., adding $1/8$ to the result obtained from Eq. (5.19), the scaling dimension is then

$$2x_{2k_b-1, 2k_g} =$$

$$\frac{1}{8} + \frac{1}{4} [(1 - e_b)(2k_b - 1)^2 + (1 - e_g)(2k_g)^2] + \quad (7.17)$$

$$- \left[\frac{e_b^2}{1 - e_b} + \frac{e_g^2}{1 - e_g} (1 - \delta_{k_g, 0}) \right].$$

F. Complete spectrum of string dimensions

Finally, the results of Eqs. (7.10), (7.12) and (7.17) can be combined into a single equation for the scaling dimension of a string operator that corresponds to s_b black loop segments and s_g grey loop segments:

$$2x_{s_b, s_g} =$$

$$\frac{1}{8} \delta_{s_b+s_g, 1}^{(2)} + \frac{1}{4} [(1 - e_b)s_b^2 + (1 - e_g)s_g^2] - \quad (7.18)$$

$$\left[\frac{e_b^2}{1 - e_b} (1 - \delta_{s_b, 0}) + \frac{e_g^2}{1 - e_g} (1 - \delta_{s_g, 0}) \right] +$$

$$\delta_{s_b, 1}^{(2)} \delta_{s_g, 1}^{(2)} \frac{(1 - e_b)(1 - e_g)}{(1 - e_b) + (1 - e_g)};$$

here we have defined $\delta_{i,j}^{(2)} \equiv \delta_{i=j \pmod{2}}$.

VIII. TERMINATION OF CRITICAL BEHAVIOUR

In the preceding sections we have developed an effective description of the critical phase of the FPL² model in the form of a field theory. This theory has to break down at large values of the loop fugacity since in this case a typical state of the model will consist of small loops only, i.e., a power-law distribution of loop sizes will be absent. That this indeed happens can be seen from the Liouville field theory itself as it carries the seeds of its own demise.

The mapping of the loop model to an oriented loop model for $n_b, n_g \leq 2$ works equally well for $n_b > 2$ or $n_g > 2$. From Eq. (4.1) it follows that in the latter case at least one of the parameters, e_b or e_g , will be pure imaginary. This affects the Liouville potential which for $n_b > 2$ or $n_g > 2$ becomes a *relevant* perturbation to the (modified) Gaussian action $S_E + S_B$.

To understand how this comes about we consider the simple case provided by the $n_b = n_g$ FPL² model, discussed in Sec. V C 2. Namely, as we increase the value of the loop fugacity we expect small loops to be favoured and the stiffness K of the interface to grow. In the critical phase this is offset by the decrease in the background charge in a way that leaves the Liouville potential marginal. Now when the loop fugacity exceeds 2 the background charge $\mathbf{e}_0 = -\pi(e_b, 0, 0)$ becomes pure imaginary and the dimension of the Liouville potential

$$x_L = \frac{\pi}{2} \frac{1 - e_b}{K} \quad (8.1)$$

can no longer stay marginal; here $x_L \equiv x(\mathbf{e}^{(i)}, 0)$, where the charges $\mathbf{e}^{(i)}$ are given in Eq. (5.24), and their scaling dimensions are calculated from Eq. (5.23). In fact, assuming that the stiffness K continues to increase with the loop fugacity for $n_b = n_g > 2$, x_L turns complex with a real part that is *smaller* than two, rendering the Liouville potential *relevant*.

If we make the usual assumption of no intervening fixed points, the relevant Liouville potential will generate a finite correlation length and the loop model will no longer be critical. The correlation length has the physical interpretation of the average size of a loop in the system. This scenario has been confirmed for the fully packed loop model on the honeycomb lattice, from the Bethe ansatz solution of this model [42].

A different view of the non-critical region of the FPL² model is provided by the locking potential $V(\mathbf{h})$. Namely, the discrete nature of the microscopic heights can be taken into account in the field theory by a negative potential in height space that is peaked around the flat, ideal states. As such, this potential is uniform on the ideal state graph and can therefore be expanded in a Fourier series. Examination of the most relevant vertex operators in this series [28] reveals that they are the same as the ones for the loop-weight (Liouville) potential, $w(\mathbf{h})$. Therefore, just like $w(\mathbf{h})$, the locking potential in the non-critical region of the phase diagram is a *relevant* perturbation. Thus, it will lock the interface in one of the ideal, flat states. In this flat phase the height fluctuations are bounded (as opposed to being logarithmically divergent) which is just another way of saying that large contour loops are exponentially suppressed. On the other hand, in the critical region of the FPL² model the locking potential is marginal as it would be for an interface model *at* the roughening transition [43]. This might indicate that the whole critical region of the FPL² model

can be understood as a manifold of essential singularities in some more general model, as was the case for the honeycomb FPL model [21,44].

As advertised in Secs. VI and VII our results for the central charge and a number of the geometrical scaling dimensions have been very accurately confirmed by transfer matrix calculations. Before turning to a discussion of our numerical results we describe the particular representation of the transfer matrix used to obtain them.

IX. CONSTRUCTION OF THE TRANSFER MATRIX

To construct the transfer matrix for the FPL² model on a cylinder of circumference L we write the partition function as

$$Z^{(M)} = \sum_{\mathcal{G}_M} n_b^{N_b} n_g^{N_g}, \quad (9.1)$$

where the length of the cylinder M has been explicitly indicated. Periodic boundary conditions are imposed in the horizontal direction, whereas the bottom and the top row of the cylinder have open boundary conditions and hence terminate in L dangling edges. We recall that the restriction of the summation to the set of fully packed graph configurations \mathcal{G}_M implies that locally the vertices are constrained to have one of the six appearances shown in Fig. 3. In the first four possible vertices the loop segments do not cross, whilst in the last two vertices the two flavours intersect. The global constraint that all loops be closed in the limit of an infinite system means that loop segments cannot terminate in the bulk but only at the dangling edges in the top and bottom rows.

A typical loop configuration for a cylinder with $L = 6$ and $M = 12$ is shown in Fig. 8. The horizontal numbering pertains to the vertices, whilst in the vertical direction it is more convenient to label each row by the number of the vertex immediately below it. Accordingly the labels 0 and M refer to the bottom and the top row of dangling edges respectively. We shall soon see that the inclusion in \mathcal{G}_M of one or more strings running between the dangling edges of row 0 and M helps us access the geometrical exponents of the model. In particular, the configuration of Fig. 8 having one such string of each flavour furnishes a contribution to the scaling dimension x_1 which determines the conformational exponent $\gamma = 1 - x_1$.

A. Connectivity basis

The construction of a transfer matrix (TM) for Eq. (9.1) appears to be obstructed by the non-locality of N_i ($i = b, g$). The key to solving this problem is to

write the TMs in a basis of *connectivity states* comprising information about how the dangling ends of row M are pairwise interconnected in the preceding rows and, if strings are present, information about the positions of such strings. In addition the connectivity states must keep track of the particular flavour of any loop or string segment terminating in row M . Our construction generalises the work of Blöte and Nightingale for the Q -state Potts model [45,46] and that of Blöte and Nienhuis for the $O(n)$ model [47] to take the extra flavour information into account, and our notation is consistent with that of these authors.

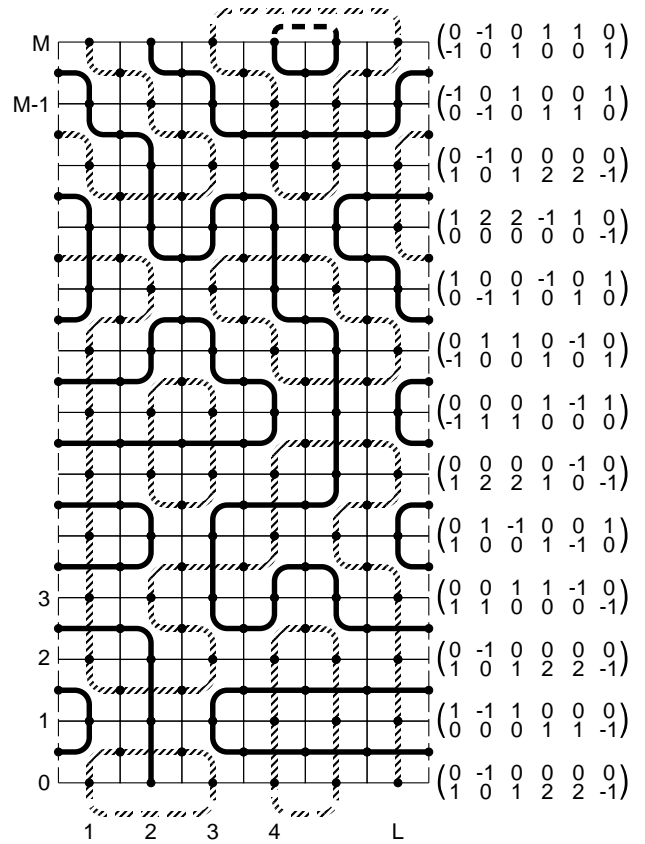


FIG. 8. A typical loop configuration for $L = 6$ and $M = 12$. The dashed lines along the left and the right boundaries illustrate the periodic boundary conditions. Horizontally the vertices are numbered from 1 to L , whilst vertically the rows are labeled by the number of the vertex immediately below them. This particular configuration is constrained to having precisely one string of each flavour spanning the length of the cylinder, and hence it contributes to the geometrical exponent x_1 . To the right we show the index representation of the connectivity state pertaining to each row (see Appendix B for details). Any valid configuration can be interpreted as a “jigsaw puzzle” assembled from the six “pieces” shown in Fig. 3. Note that when laying down the first row of this puzzle it must be stipulated how the dangling edges of row 0, which are not part of a string, are pairwise interconnected below that row. These implicit connections as well as their counterparts in row M have been depicted by dashed loop segments.

It is essential to be able to represent a given connectivity state both in an *index representation* giving direct access to the flavour and connectedness information just mentioned, and in a *number representation* assigning an integer in the range $1, 2, \dots, C_L^{(s_b, s_g)}$ to the state under consideration. The latter representation enables us to enumerate the entries of the TM, whilst the former allows us to determine the number of loop closures when going from one connectivity state to another and hence the value of a particular entry in the TM. Here $C_L^{(s_b, s_g)}$ is the number of distinct connectivity states for a cylinder of width L accommodating s_i strings of flavour $i = b, g$. The construction of these two representations, the mapping between them, and the evaluation of the $C_L^{(s_b, s_g)}$ for $(s_b, s_g) = (0, 0), (1, 0), (1, 1)$ and $(2, 0)$ is deferred to Appendix B.

Designating the connectivity states by Greek letters we can write the partition function as a sum of restricted partition functions

$$Z^{(M)} = \sum_{\beta} Z_{\beta}^{(M)} = \sum_{\beta} \sum_{\mathcal{G}_M} \delta(\beta, \phi(\mathcal{G}_M)) n_b^{N_b} n_g^{N_g}, \quad (9.2)$$

where $\phi(\mathcal{G}_M)$ is the connectivity of the L dangling edges of row M , and $\delta(i, j)$ is the Kronecker delta. Now consider appending another row to the cylinder, giving us a total graph configuration $\mathcal{G}_{M+1} = \mathcal{G}_M \cup \mathcal{G}'$. Evidently

the connectivity of the dangling edges of row $M + 1$ is determined solely by that of the preceding row and by the appended subgraph \mathcal{G}'

$$\phi(\mathcal{G}_{M+1}) = \psi(\phi(\mathcal{G}_M), \mathcal{G}'). \quad (9.3)$$

Letting N'_i denote the number of loop closures induced by \mathcal{G}' we arrive at the relation

$$\begin{aligned} Z_\alpha^{(M+1)} &= \sum_{\mathcal{G}_{M+1}} \delta(\alpha, \phi(\mathcal{G}_{M+1})) n_b^{N_b+N'_b} n_g^{N_g+N'_g} \\ &= \sum_{\beta} \sum_{\mathcal{G}_M} \delta(\beta, \phi(\mathcal{G}_M)) n_b^{N_b} n_g^{N_g} \\ &\quad \sum_{\mathcal{G}'|\mathcal{G}_M} \delta(\alpha, \psi(\phi(\mathcal{G}_M), \mathcal{G}')) n_b^{N'_b} n_g^{N'_g} \\ &= \sum_{\beta} T_{\alpha\beta} Z_\beta^{(M)}, \end{aligned} \quad (9.4)$$

where the transfer matrix is defined by

$$T_{\alpha\beta} = \sum_{\mathcal{G}'|\mathcal{G}_M} \delta(\alpha, \psi(\phi(\mathcal{G}_M), \mathcal{G}')) n_b^{N'_b} n_g^{N'_g}. \quad (9.5)$$

The notation $\mathcal{G}'|\mathcal{G}_M$ means that the summation is constrained to those subgraphs \mathcal{G}' that fit the dangling edges of \mathcal{G}_M .

B. Single-vertex decomposition

A quintessential step in the practical implementation of the TM is its decomposition into matrices each corresponding to the addition of a single vertex,

$$\mathbf{T} = \mathbf{T}_L \cdot \mathbf{T}_{L-1} \cdot \dots \cdot \mathbf{T}_1. \quad (9.6)$$

Here the single-vertex matrix \mathbf{T}_i , which adds the vertex at horizontal position i of the new row, has the advantage of being *sparse*, and we shall soon see that it has at most three non-zero entries per column. This property leads to a dramatical reduction of the time and storage requirements for the calculations.

As was the case in the $O(n)$ model [47], a minor complication arises due to the fact that the addition of the first vertex of a new row increases the number of dangling edges from L to $L + 2$. This is illustrated in the left part of Fig. 9. Upon addition of further vertices the number of dangling edges is kept fixed at $L + 2$, until the L 'th vertex completes the row, and we are back at L dangling edges. Thus the dimensions of the single-vertex matrices are $C_{L+2} \times C_L$ for \mathbf{T}_1 , $C_{L+2} \times C_{L+2}$ for $\mathbf{T}_2, \dots, \mathbf{T}_{L-1}$, and $C_L \times C_{L+2}$ for \mathbf{T}_L .

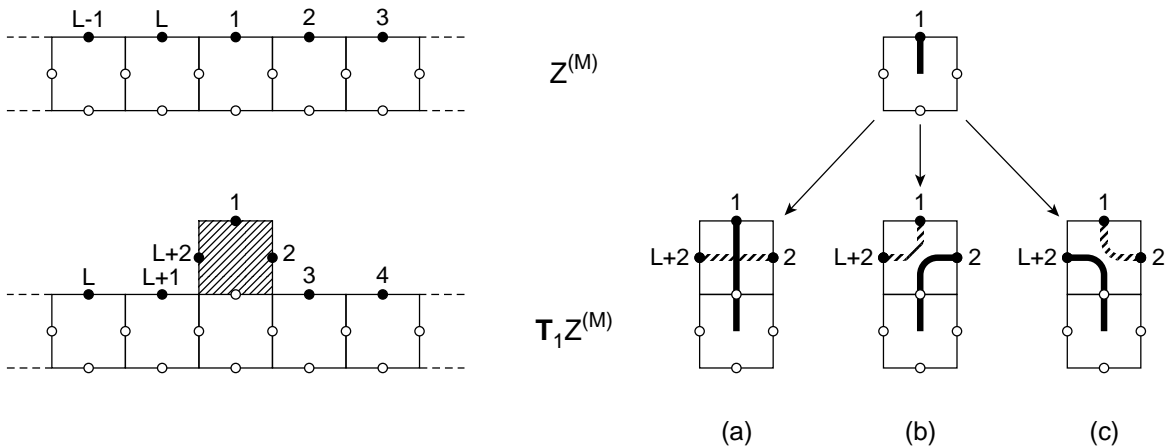


FIG. 9. Adding the first vertex of the $(M + 1)$ 'th row increases the number of dangling edges from L to $L + 2$. The labeling of the “active” edges (filled circles) before and after addition of the new vertex (shaded) is as shown in the left part of the figure. The part of the lattice relevant for determining which of the vertices of Fig. 3 fit onto a given connectivity of row M , has been depicted in the right part of the figure. This information constitutes the *vertex rules*, and is explained in the text.

In Fig. 9 we illustrate the action of \mathbf{T}_1 on $Z^{(M)}$ in detail. To ensure that row $M + 1$, when completed, will have the same labels on its dangling edges as was the case in the preceding row, the solid dots illustrating the “active” dangling edges must be relabeled as shown in the lower left part of the figure. Shown to the right are the three possible choices of vertices fitting onto a black

loop segment terminating at the dangling end 1 of $Z^{(M)}$. There are thus three non-zero entries in each column of \mathbf{T}_1 . Since no loop closures of either flavour can be induced ($N'_b = N'_g = 0$ in Eq. (9.5)) all these entries are unity. Similar considerations hold true when the loop segment to be fitted is grey, and the vertex rules can be read off from the figure by interchanging the two flavours.

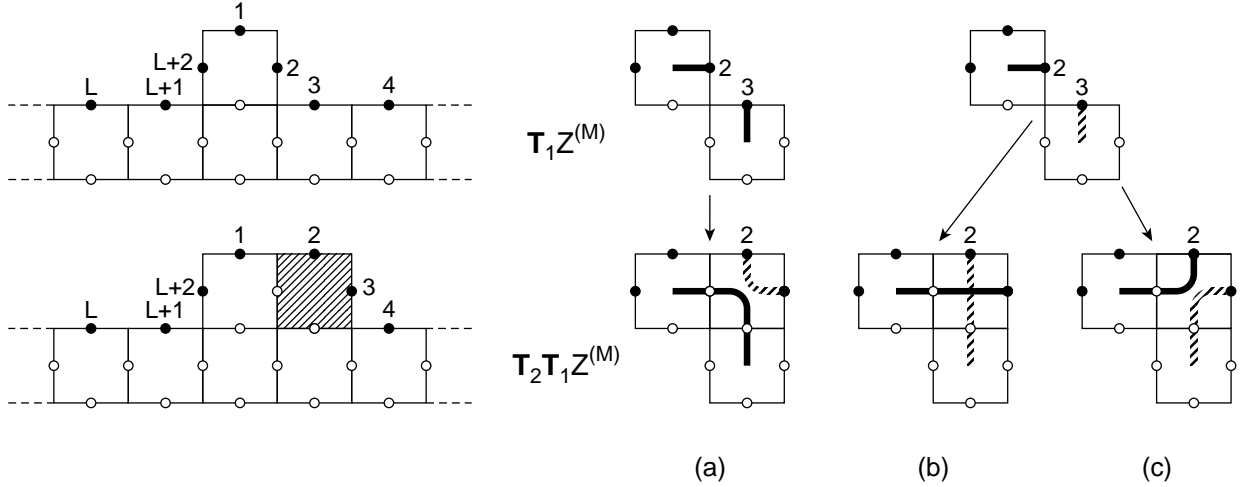


FIG. 10. Addition of subsequent vertices keeps the number of dangling edges fixed at $L + 2$. In the left part of the figure the system is shown before and after the addition of the second vertex (shaded). Vertex rules are displayed to the right. Situation (a) allows for the possibility of a black loop closure.

When acting with any one of the subsequent single-vertex TMs $\mathbf{T}_2, \dots, \mathbf{T}_{L-1}$ the situation is as depicted in Fig. 10 for the case of \mathbf{T}_2 . As the number of dangling edges is kept fixed no relabeling is needed, apart from the translation of labels 2 and 3 up on top of the newly added vertex. The vertex rules for the case where edge 2 of $\mathbf{T}_1 Z^{(M)}$ is black are shown in the right part of the figure; similar rules for the case where it is grey can be obtained by permuting the two flavours.

In situation (a) only one vertex fits onto the two dangling edges. The column of \mathbf{T}_2 determined by the number representation of the connectivity pertaining to the $L + 2$ dangling ends that are active in the upper part of the figure thus has only one non-zero entry. Its value is either n_b or 1 depending on whether a black loop closure is

induced ($i_2^b = i_3^b$) or not ($i_2^b \neq i_3^b$). In the index representation of the new connectivity state $i_2^g = i_3^g$ is set equal to a positive integer not assumed by any other i_k^g . The new values of the black indices depend on whether a loop closure is induced or not. In the former case we simply set $i_2^b = i_3^b = 0$. In the latter, the two left-over black partners must be mutually connected before assigning $i_2^b = i_3^b = 0$.

Situations (b) and (c) correspond to two entries of each column of \mathbf{T}_2 taking the value unity, the others being zero. Since loop closures are out of the question the handling of these cases is simple. In (b) the two flavours cross, and the indices of sites 2 and 3 are interchanged. Case (c) is even simpler: it corresponds to a diagonal entry in \mathbf{T}_2 .

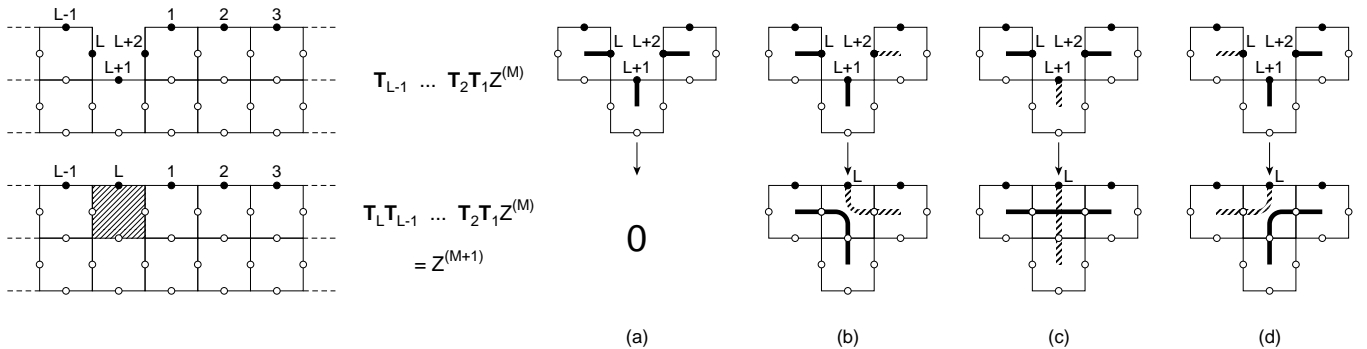


FIG. 11. Completing the $(M + 1)$ 'th row by adding the L 'th vertex (shaded) brings the number of dangling edges back to L . The labeling is now consistent with that of the preceding rows. Vertex rules, shown to the right, now include a disallowed configuration. Namely, in situation (a) none of the vertices of Fig. 3 fit in, and the corresponding entry of the transfer matrix must be forced to zero. Situations (b), (c) and (d) offer various possibilities for a black loop closure.

When strings are present a few modifications of the above rules are necessary. In situation (a), if one of i_2^b and i_3^b equals -1 and the other is positive, the left-over partner to the non-string black segment must be made the new string. And if both i_2^b and i_3^b equal -1 the corresponding entry of \mathbf{T}_2 must be forced to zero, since two strings cannot be allowed to annihilate.

Finally, consider closing the $(M + 1)$ 'th row through the action of \mathbf{T}_L , as depicted in Fig. 11. The labels $L + 1$ and $L + 2$ now disappear, and as far as the labeling goes the system is back in its original state. Each column of \mathbf{T}_L has at most one non-zero entry per column, as witnessed by the vertex rules displayed in the right part of the figure. Once again, only half of the vertex rules are shown, and the other half is found by interchanging the two flavours.

In situation (a) no vertex of Fig. 3 can fit onto the three dangling edges at positions L , $L + 1$ and $L + 2$. The corresponding entry of \mathbf{T}_L must therefore be forced to zero. Situations (b), (c) and (d) leave us to determine whether, for a given connectivity of the $L + 2$ dangling edges, a black loop closure occurs or not. The handling in terms of the index representation is exactly as described above.

X. NUMERICAL RESULTS

A. Central charge

The reduced free energy per vertex in the limit $M \rightarrow \infty$ of an infinitely long cylinder is given by

$$f_0^{(0,0)}(L) = \lim_{M \rightarrow \infty} \frac{1}{LM} \ln \text{Tr} Z^{(M)} = -\frac{1}{L} \ln \lambda_0^{(0,0)}, \quad (10.1)$$

where $\lambda_0^{(s_b, s_g)}$ is the largest eigenvalue of $\mathbf{T}^{(s_b, s_g)}$. The partition function for a cylinder of length M is found by iterating the no-string TM

$$Z^{(M)} = \left(\mathbf{T}^{(0,0)} \right)^M Z^{(0)}. \quad (10.2)$$

It is well-known that conformal invariance relates the amplitude of the $1/L^2$ corrections to $f_0^{(0,0)}(\infty)$ to the central charge c [37]. A further (non-universal) $1/L^4$ correction due to the operator $T\bar{T}$, where T denotes the stress tensor, must also be present in any conformally invariant system [48]. It is therefore found in a number of cases [45,49,50] that fits of the form

$$f_0^{(0,0)}(L) = f_0^{(0,0)}(\infty) - \frac{\pi c}{6L^2} + \frac{A}{L^4} \quad (10.3)$$

yield very rapidly converging estimates for c . An efficient application of Eq. (10.3) is to determine c from parabolic least-squares fits of the finite-size data against $1/L^2$ [49,50].

In Table I the results of such fits including the data points for $L_0 \leq L \leq L_{\max}$ are shown as a function of L_0 . Numerically we were able to access $L_{\max} = 14$, in which case the largest single-vertex TMs have dimension $\sim 7 \cdot 10^6$ (see Table VII). The extrapolation of the estimants $c(L_0, L_{\max})$ to the limit of infinite L_0 is assumed to take the form of a power law

$$c(L_0, L_{\max}) = c + kL_0^{-p}, \quad (10.4)$$

at least within an asymptotic regime of large enough L_0 . As is evident from Table I the last three estimants usually exhibit monotonicity, thus allowing us to fix the constants c , k and p . When this was not the case, or whenever the power p thus obtained was too small to produce a reliable extrapolation the Ising-like value $p = 2$ was used by default to extrapolate the last two estimants. An error bar for this type of fit can be estimated from the variation among the individual estimants. The extrapolants are invariably in excellent agreement with our analytical results, the relative deviation being typically of the order 10^{-3} .

n_b	n_g	$c(4, 14)$	$c(6, 14)$	$c(8, 14)$	$c(10, 14)$	Extrapolation	Exact
0.0	0.0	-2.8943	-2.8861	-2.9220	-2.9514	-3.0037	-3.0000
0.5	0.0	-1.8528	-1.7641	-1.7716	-1.7873	-1.8152	-1.8197
0.5	0.5	-0.7295	-0.6249	-0.6159	-0.6220	-0.6328	-0.6395
1.0	0.0	-1.0012	-0.9542	-0.9636	-0.9761	-0.9983	-1.0000
1.0	0.5	0.1341	0.1877	0.1924	0.1895	0.1843	0.1803
1.0	1.0	0.9918	0.9969	0.9986	0.9999	1.0004	1.0000
1.5	0.0	-0.3765	-0.3669	-0.3817	-0.3923	-0.4111	-0.4124
1.5	0.5	0.7652	0.7746	0.7729	0.7715	0.7690	0.7678
1.5	1.0	1.6215	1.5818	1.5778	1.5806	1.5856	1.5876
1.5	1.5	2.2541	2.1691	2.1581	2.1627	2.1709	2.1751
2.0	0.0	0.0706	0.0549	0.0342	0.0235	-0.0019	0.0000
2.0	0.5	1.2209	1.1937	1.1868	1.1861	1.1849	1.1803
2.0	1.0	2.0792	2.0002	1.9899	1.9937	2.0005	2.0000
2.0	1.5	2.7139	2.5919	2.5737	2.5781	2.5859	2.5876

2.0	2.0	3.1629	3.0121	2.9885	2.9936	3.0027	3.0000
-----	-----	--------	--------	--------	--------	--------	--------

TABLE I. Estimants $c(L_0, L_{\max})$ for the central charge are obtained from parabolic least-squares fits against $1/L^2$ using the numerical data for $L_0 \leq L \leq L_{\max}$. The extrapolation in L_0 is described in the text.

The results for c are shown for all integer and half-integer values of $n_i \in [0, 2]$. Because of the symmetric appearance of the two flavours in Eq. (9.1) only $n_b \geq n_g$ need be considered. For either $n_b = 1$ or $n_g = 1$ the FPL² model reduces to the simpler FPL model earlier considered by Batchelor *et al.* [14], and for $n_b = n_g$ we recover another special case recently investigated by one of us [7].

B. Thermal scaling dimension

A further prediction of conformal invariance is that the finite-size scaling of the first gap in the eigenvalue spectrum of $\mathbf{T}^{(0,0)}$ is related to the thermal scaling dimension [38]

$$f_1^{(0,0)}(L) - f_0^{(0,0)}(L) = \frac{2\pi x_T}{L^2} + \dots, \quad (10.5)$$

where $f_1^{(0,0)}$ is found from the next-largest eigenvalue of $\mathbf{T}^{(0,0)}$ through $f_1^{(0,0)} = -\frac{1}{L} \ln \lambda_1^{(0,0)}$. These computations

were also carried through for even L up to $L_{\max} = 14$. In this case as well the convergence of the estimants can be considerably sped up by including a $1/L^4$ term in Eq. (10.5) and performing parabolic least-squares fits versus $1/L^2$.

The results for x_T as displayed in Table II again agree with those of the previously studied special cases [14,7]. The data for $(n_b, n_g) = (0, 0)$ merit a special comment. Monitoring the three leading eigenvalues $\lambda_0^{(0,0)}$, $\lambda_1^{(0,0)}$ and $\lambda_2^{(0,0)}$ as a function of n for $n_b = n_g \equiv n$ we found that $\lambda_1^{(0,0)}$ and $\lambda_2^{(0,0)}$ are exactly degenerate for all n down to $n \sim 0.20$. Hereafter $\lambda_1^{(0,0)}$ splits off from $\lambda_2^{(0,0)}$ and eventually becomes degenerate with $\lambda_0^{(0,0)}$ at $n = 0$. Because of this level crossing it thus seems very likely that near $(n_1, n_2) = (0, 0)$ the thermal eigenvalue should be related to the gap $f_2^{(0,0)}(L) - f_0^{(0,0)}(L)$. Comparison with the exactly known result $x_T = 1/2$ [7] confirms this suspicion. A similar comment holds true near $(n_b, n_g) = (2, 2)$, and again we find fair agreement with the exact result if we apply Eq. (10.5) to $\lambda_2^{(0,0)}$, and not to $\lambda_1^{(0,0)}$ (which in this case becomes two-fold degenerate).

n_b	n_g	$x_T(4, 14)$	$x_T(6, 14)$	$x_T(8, 14)$	$x_T(10, 14)$	Extrapolation	Ref. [14]	Exact
0.0	0.0	0.5712	0.5280	0.5121	0.5060	0.4987		0.5000
0.5	0.0	0.5704	0.5535	0.5452	0.5417	0.5366		0.5372
0.5	0.5	0.5916	0.5882	0.5845	0.5825	0.5789		0.5804
1.0	0.0	0.5826	0.5798	0.5765	0.5748	0.5708	0.573 (1)	0.5714
1.0	0.5	0.6204	0.6227	0.6218	0.6211	0.6199	0.6200 (5)	0.6206
1.0	1.0	0.66368	0.66600	0.66642	0.66654	0.66663	0.6666 (1)	0.66667
1.5	0.0	0.5965	0.6053	0.6060	0.6058	0.6054		0.6063
1.5	0.5	0.6493	0.6559	0.6574	0.6578	0.6585		0.6619
1.5	1.0	0.7782	0.7094	0.7108	0.7115	0.7130	0.713 (1)	0.7146
1.5	1.5	0.8950	0.7657	0.7674	0.7684	0.7702		0.7699
2.0	0.0	0.6167	0.6295	0.6338	0.6349	0.6356		0.6667
2.0	0.5	0.7481	0.6878	0.6913	0.6927	0.6945		0.7345
2.0	1.0	0.8741	0.7566	0.7552	0.7565	0.7588	0.76 (1)	0.8000
2.0	1.5	0.9436	0.8755	0.8284	0.8303	0.8337		0.8702
2.0	2.0	0.9996	0.9850	0.9400	0.9200	0.8876		1.0000

TABLE II. The thermal scaling dimension x_T . The extrapolation of the estimants $x_T(L_0, L_{\max})$ is described in the text. For comparison we also show the numerical data for the case of either n_b or n_g being unity [14]. Due to level crossing the values of x_T for $(n_b, n_g) = (0, 0)$ and $(2, 2)$ are found from the gap $f_2^{(0,0)}(L) - f_0^{(0,0)}(L)$ rather than from $f_1^{(0,0)}(L) - f_0^{(0,0)}(L)$.

For $n_b < 2$ the extrapolants are again in excellent ($\sim 10^{-3}$ or better) agreement with our analytical results. For $n_b = 2$ the slower convergence can be attributed to logarithmic corrections [51] arising from an enhanced number of marginal vertex operators. Indeed,

of the twelve vertex operators corresponding to the shortest vectors in \mathcal{R}_w^* , Eq. (5.18), seven stay marginal when either $n_b < 2$ or $n_g < 2$. In the general case, when both $n_b < 2$ and $n_g < 2$, there are only four marginal vertex operators; this is the loop ansatz, Eq. (5.25).

C. Dimensions of string operators

We now turn our attention to the determination of the scaling dimensions associated with one or more strings spanning the length of the cylinder. The presence of one black string corresponds to a height mismatch in the ideal states, and the relevant scaling dimension X is therefore that of a *twist-like operator* [41]. We have calculated the leading eigenvalue of $\mathbf{T}^{(1,0)}$ for odd system sizes up to $L_{\max} = 13$ and determined the corresponding estimants $c_{\text{odd}}(L_0, L_{\max})$ by the usual parabolic fits to $f_0^{(1,0)}(L)$, cfr. Eq. (10.3). Estimants $X(L_0, L_{\max})$ are then defined by

$$X(L_0, L_{\max}) = \frac{c - c_{\text{odd}}(L_0, L_{\max})}{12}, \quad (10.6)$$

where the factor of 12 originates from a comparison of Eq. (10.3) with Eq. (10.5). For the central charge c of an even-sized system we use our analytical results, Eq. (6.4).

These estimants and their extrapolations are found in Table III. Note that we can no longer limit the parameter values by $n_b \geq n_g$, as the condition $(s_b, s_g) = (1, 0)$

treats the two flavours asymmetrically. In the case of the FPL model ($n_b = 1$) it was found [14] that X was independent of n_g . It is evident from our numerical data that this n_g -independence in fact pertains to all $n_b \in [0, 2]$. Final results for X as a function of n_b have therefore been computed by averaging the available extrapolated scaling dimensions over n_g . For $n_b = 1$ the agreement with the result $X \approx 1/8$ found by Batchelor *et al.* [14] is excellent. Furthermore we are able to conjecture the general formula, Eq. (7.15), for X as a function of the loop fugacities.

When $(s_b, s_g) = (1, 1)$ the parity of L must again be even, and we can make parabolic fits for the gap $f_0^{(1,1)}(L) - f_0^{(0,0)}(L)$, as in Eq. (10.5), without taking resort to the less accurate method of fitting for two central charges separately as above. The corresponding universal amplitude is identified with the scaling dimension x_1 . The results, now for $L_{\max} = 12$, are shown in Table IV, and our values for the scaling dimension are once again in agreement with the analytical results, apart from $n_g = 2$ where logarithmic corrections are the most likely source of systematic errors [51].

n_b	n_g	$X(3, 13)$	$X(5, 13)$	$X(7, 13)$	$X(9, 13)$	Extrapolation	Result	Exact
0.0	0.0	-0.05586	-0.06109	-0.06203	-0.06232	-0.06257	-0.06269 (31)	-0.06250
0.0	0.5	-0.06080	-0.06197	-0.06220	-0.06233	-0.06253		-0.06250
0.0	1.0	-0.06043	-0.06198	-0.06221	-0.06233	-0.06250		-0.06250
0.0	1.5	-0.05869	-0.06156	-0.06215	-0.06233	-0.06259		-0.06250
0.0	2.0	-0.05804	-0.06190	-0.06297	-0.06316	-0.06324		-0.06250
0.5	0.0	0.04674	0.04538	0.04558	0.04569	0.04587	0.04583 (16)	0.04591
0.5	0.5	0.04572	0.04585	0.04589	0.04588	0.04588		0.04591
0.5	1.0	0.04643	0.04622	0.04614	0.04607	0.04595		0.04591
0.5	1.5	0.04781	0.04675	0.04638	0.04622	0.04590		0.04591
0.5	2.0	0.04828	0.04664	0.04593	0.04573	0.04555		0.04591
1.0	0.0	0.11895	0.12278	0.12398	0.12438	0.12501	0.12497 (8)	0.12500
1.0	0.5	0.12346	0.12422	0.12458	0.12470	0.12489		0.12500
1.0	1.0	0.12465	0.12485	0.12495	0.12496	0.12498		0.12500
1.0	1.5	0.12584	0.12540	0.12529	0.12521	0.12508		0.12500
1.0	2.0	0.12652	0.12549	0.12513	0.12501	0.12490		0.12500
1.5	0.0	0.17106	0.18253	0.18453	0.18536	0.18662	0.18663 (25)	0.18687
1.5	0.5	0.18283	0.18468	0.18553	0.18585	0.18633		0.18687
1.5	1.0	0.18515	0.18588	0.18620	0.18632	0.18646		0.18687
1.5	1.5	0.18684	0.18684	0.18687	0.18684	0.18680		0.18687
1.5	2.0	0.18878	0.18796	0.18759	0.18741	0.18696		0.18687
2.0	0.0	0.2076	0.2296	0.2321	0.2340	0.2369	0.2392 (27)	0.2500
2.0	0.5	0.2283	0.2323	0.2342	0.2351	0.2371		0.2500
2.0	1.0	0.2325	0.2347	0.2358	0.2363	0.2383		0.2500
2.0	1.5	0.2357	0.2372	0.2379	0.2383	0.2400		0.2500
2.0	2.0	0.2402	0.2413	0.2417	0.2420	0.2435		0.2500

TABLE III. Estimants $X(L_0, L_{\max})$ for the scaling dimension of the twist operator along with their extrapolations to the infinite-system limit. For $n_b = 1$ the value $X = 1/8$ was previously found to be independent of n_g [14]. It is evident that this n_g -independence holds for any value of n_b , and in accordance herewith our final result is obtained by averaging the various extrapolants over n_g .

Finally, the results for x_2 as obtained from parabolic fits for the gap $f_0^{(2,0)}(L) - f_0^{(0,0)}(L)$ are shown in Table V. Again we have $L_{\max} = 12$. Just like in the case of X we find the extrapolated values of x_2 to be independent of n_g , and final results are obtained by averaging over this parameter.

D. Entropy

Apart from the various universal quantities, such as the central charge and the scaling dimensions, the transfer matrices also provide numerical values for the residual entropy per vertex, $s = f_0(\infty)$. In the limit $n_g \rightarrow 0$ of compact polymers this quantity is of interest to the protein folding community, due to the fact that native conformations of all globular proteins are compact [5].

Using our knowledge of the exact form of the finite-size corrections of order $1/L^2$, Eq. (10.3), we have obtained

very accurate extrapolations to the limit of an infinite system.⁶ After subtracting the $1/L^2$ correction a series of estimants $s(L, L_{\max})$ may be obtained by fitting the residual size dependence to a pure $1/L^4$ form. The remaining L -dependence of these estimants turns out to be well accounted for by a further $1/L^4$ fit, and in this way we arrive at a final value for s . The error bar on the final value can be estimated as its deviation from the most accurate extrapolant, $s(L_{\max} - 2, L_{\max})$.

The most accurate results are quite naturally found by employing this procedure on $f_0^{(0,0)}(L)$, and they are shown in Table VI. Results obtained by extrapolating the free energies for other sectors of the transfer matrix containing strings are consistent herewith but have error bars that are roughly 10 times larger. If the fugacity of one of the strings equals two the error bars are even larger, which is to be anticipated from the fact that logarithmic corrections to the scaling dimensions are larger than similar corrections to the central charge [51].

n_b	n_g	$x_1(4, 12)$	$x_1(6, 12)$	$x_1(8, 12)$	Extrapolation	Ref. [14]	Exact
0.0	0.0	-0.2433	-0.2447	-0.2470	-0.2500		-0.2500
0.5	0.0	-0.1328	-0.1295	-0.1303	-0.1313		-0.1323
0.5	0.5	-0.01713	-0.01228	-0.01217	-0.01217		-0.0131
1.0	0.0	-0.0440	-0.0423	-0.0430	-0.0439	-0.0444 (1)	-0.0446
1.0	0.5	0.0737	0.0763	0.0764	0.0765	0.0750 (3)	0.0761
1.0	1.0	0.16608	0.16646	0.16657	0.16663	0.1667 (1)	0.16667
1.5	0.0	0.0267	0.0271	0.0264	0.0255		0.0260
1.5	0.5	0.1466	0.1472	0.1472	0.1472		0.1483
1.5	1.0	0.2411	0.2395	0.2395	0.2394	0.242 (2)	0.2405
1.5	1.5	0.3196	0.3159	0.3156	0.3156		0.3162
2.0	0.0	0.0845	0.0848	0.0844	0.0839		0.1042
2.0	0.5	0.2070	0.2067	0.2071	0.2076		0.2295
2.0	1.0	0.3048	0.3021	0.3024	0.3028	0.307 (2)	0.3250
2.0	1.5	0.3882	0.3841	0.3842	0.3843		0.4044
2.0	2.0	0.4640	0.4618	0.4635	0.4657		0.5000

TABLE IV. Scaling dimension x_1 , corresponding to one string of each flavour.

In the special case of the equal-weighted six-vertex model, $(n_b, n_g) = (1, 1)$, our value for s is in excellent agreement with the exact result due to Lieb [52],

$$s(1, 1) = \frac{3}{2} \ln \left(\frac{4}{3} \right) \simeq 0.4315231 \dots, \quad (10.7)$$

and in the limit of two mutually excluding Hamiltonian walks, $(n_b, n_g) = (0, 0)$, we are able to conjecture the result

$$s(0, 0) = \frac{1}{2} \ln(2) \simeq 0.3465735 \dots \quad (10.8)$$

In fact, after having made this conjecture we discovered that the numerical values of $f_0^{(1,1)}(L)$, i.e., the free energy per site in the sector where we enforce one string of each flavour, are *independent* of L for $4 \leq L \leq 12$, and equal to $\frac{1}{2} \ln(2)$ with full 16-digit machine precision. Since the

⁶The logarithmic corrections to the free energy implied by the $\mathcal{N}^{\gamma-1}$ term in Eq. (2.6) does not pertain to the cylindrical geometry implicit in our transfer matrix calculations. A similar remark applies to the surface term $\kappa_s^{\mathcal{N}^{(d-1)/d}}$.

free energy per site in the thermodynamic limit is unchanged by the introduction of a string defect, this observation lends credibility to the correctness of the above conjecture.

Our result in the compact polymer limit merits special attention. Traditionally the entropy is quoted in terms of the so-called connective constant $\kappa = e^{s(1,0)}$; see Eq. (2.6). Early approximations due to Flory [53] and Huggins [54] yielded respectively

$$\kappa_{\text{Flory}} = \frac{z-1}{e} \simeq 1.104 \quad (10.9)$$

and

$$\kappa_{\text{Huggins}} = (z-1) \left(1 - \frac{2}{z}\right)^{z/2-1} = \frac{3}{2}. \quad (10.10)$$

Here $z = 4$ is the coordination number of the square lattice. More recently, $\kappa \simeq 1.472$ was found from transfer matrix calculations [26] and $\kappa = 1.475(15)$ by exhaustive computer enumeration of short-chain configurations [4]. Both these results are very close to the mean-field value $\kappa_{\text{MF}} = \frac{z}{e} = 1.4715 \dots$ [24], and it is tempting to conclude that conformations of compact polymers are in fact described by mean-field theory [4]. However, our result

$$\kappa = 1.472801(10) \quad (10.11)$$

demonstrates that this is not the case.

XI. DISCUSSION

From the construction of the effective field theory of the FPL² model some rather general conclusions regarding the scaling of compact polymers, and the relation between loop models and conformal field theory can be drawn. It also provides new insights into the three-state Potts antiferromagnet and the dimer loop model, which are identified with specific points in the phase diagram of the FPL² model. We conclude the paper with a discussion of these topics.

A. Compact polymers

One of the main motivations for studying fully packed loop models is provided by compact polymers, their scaling properties in particular. Just like polymers in the dilute and dense phase, compact polymers form a critical geometrical system characterised by conformational exponents γ and ν . The exponent γ relates the number of conformations of the polymer to the number of monomers; see Sec. II for details. The other conformational exponent (ν) relates the linear size of the polymer to the number of monomers. For compact structures it has the trivial value 1/2 since these polymers are space filling.

n_b	n_g	$x_2(4, 12)$	$x_2(6, 12)$	$x_2(8, 12)$	Extrapolation	Result	Exact
0.0	0.0	0.0000	0.0000	0.0000	0.0000	0.0000 (0)	0.0000
0.0	0.5	0.0000	0.0000	0.0000	0.0000		0.0000
0.0	1.0	0.0000	0.0000	0.0000	0.0000		0.0000
0.0	1.5	0.0000	0.0000	0.0000	0.0000		0.0000
0.0	2.0	0.0000	0.0000	0.0000	0.0000		0.0000
0.5	0.0	0.1279	0.1355	0.1372	0.1389	0.1386 (2)	0.1386
0.5	0.5	0.1365	0.1371	0.1378	0.1387		0.1386
0.5	1.0	0.1377	0.1374	0.1379	0.1385		0.1386
0.5	1.5	0.1383	0.1375	0.1379	0.1384		0.1386
0.5	2.0	0.1392	0.1376	0.1379	0.1383		0.1386
1.0	0.0	0.2333	0.2447	0.2472	0.2504	0.2495 (5)	0.2500
1.0	0.5	0.2488	0.2477	0.2484	0.2493		0.2500
1.0	1.0	0.2514	0.2487	0.2490	0.2494		0.2500
1.0	1.5	0.2538	0.2497	0.2495	0.2492		0.2500
1.0	2.0	0.2573	0.2512	0.2504	0.2494		0.2500
1.5	0.0	0.3197	0.3377	0.3416	0.3466	0.3487 (26)	0.3506
1.5	0.5	0.3429	0.3425	0.3443	0.3466		0.3506
1.5	1.0	0.3486	0.3457	0.3466	0.3478		0.3506
1.5	1.5	0.3548	0.3497	0.3496	0.3494		0.3506
1.5	2.0	0.3636	0.3561	0.3547	0.3529		0.3506
2.0	0.0	0.3920	0.4202	0.4268	0.4353	0.446 (12)	0.5000
2.0	0.5	0.4244	0.4277	0.4323	0.4382		0.5000
2.0	1.0	0.4346	0.4348	0.4382	0.4426		0.5000
2.0	1.5	0.4468	0.4452	0.4474	0.4502		0.5000
2.0	2.0	0.4640	0.4618	0.4635	0.4657		0.5000

TABLE V. Scaling dimension x_2 , corresponding to two black strings.

Prior to our work, exact results have been obtained for compact polymers on the Manhattan [55] and the honeycomb [20] lattice, and the mean-field value $\gamma = 1$ was found in both cases. This value of γ indicates that the two ends of the compact polymer are independent at large distances. This follows from the scaling relation $x_1 = 1 - \gamma = 0$, where the one-string dimension x_1 describes the probability $G_1(r) \sim r^{-2x_1}$ that the two chain ends are separated by a distance r . In this regard the scaling of compact polymers on the Manhattan and the honeycomb lattices is equivalent to that of ideal chains. Ideal chain configurations are described by simple random walks for which each step is independent of the previous one.

Here we have calculated the exact conformational exponent $\gamma = 117/112$ for compact polymers on the square lattice. The fact that $\gamma > 1$ is tantamount to an effective *repulsion* between the ends of the chain, indicating non-ideal behaviour. Indeed, the fact that the connective constant κ in Eq. (10.11) is larger than its mean-field value indicates that the origin of this repulsion is *entropic*. Earlier numerical studies of this problem utilising direct enumerations of chain conformations have failed to see any deviation from the ideal chain result $\gamma_{\text{MF}} = 1$ [4]; we can attribute this to the fact that the actual difference is indeed very small ($\gamma - \gamma_{\text{MF}} = 5/112$) and below the numerical accuracy previously achieved. The same

comment can be made for the connective constant.

Another interesting aspect of compact polymers is that their scaling properties are lattice dependent. This is in contrast to the dilute and dense case which are described by conformational exponents that do not depend on the lattice type (e.g., honeycomb *versus* square). As remarked earlier this “lack of universality” is due to a kind of geometrical frustration that arises from the fully packing constraint imposed on the loop models which are employed in studies of compact polymers.

Finally, the field theory solution of the FPL² model uncovered a property of compact polymers that, to our knowledge, was not previously anticipated. The fact that there is a whole line of critical points in this loop model in the Hamiltonian walk limit ($n_b \rightarrow 0$) indicates a continuum of universality classes described by compact polymers on the square lattice. In particular the exponent γ can be changed continuously by adjusting the fugacity of the loops uncovered by the polymer. The loop weight of the uncovered (grey) loops can be thought of as an effective interaction amongst the monomers, albeit a non-local one. A similar effect of interactions on directed self-avoiding walks was discovered by Cardy [30] from a field theoretical analysis of the problem. The existence of a continuously varying γ in this case was recently challenged by numerical results [31].

n_b	n_g	$f_0^{(0,0)}(4)$	$f_0^{(0,0)}(6)$	$f_0^{(0,0)}(8)$	$f_0^{(0,0)}(10)$	$f_0^{(0,0)}(12)$	$f_0^{(0,0)}(14)$	s
0.0	0.0	0.17328680	0.28881133	0.31784496	0.32923359	0.33490107	0.33815371	0.346575 (14)
0.5	0.0	0.26740000	0.33317928	0.35057672	0.35745438	0.36088114	0.36284872	0.367950 (9)
0.5	0.5	0.35063553	0.37668215	0.38371283	0.38639599	0.38769210	0.38842126	0.390258 (3)
1.0	0.0	0.32923947	0.36764369	0.37752555	0.38137032	0.38327066	0.38435762	0.387166 (7)
1.0	0.5	0.40772622	0.41103439	0.41126990	0.41111188	0.41095017	0.41082815	0.410405 (2)
1.0	1.0	0.46298939	0.44576535	0.43960110	0.43671524	0.43513763	0.43418273	0.4315233 (4)
1.5	0.0	0.37601935	0.39599984	0.40063320	0.40233073	0.40314475	0.40360330	0.404771 (5)
1.5	0.5	0.45180855	0.43964968	0.43509788	0.43291844	0.43171625	0.43098591	0.4289459 (10)
1.5	1.0	0.50624745	0.47501911	0.46431698	0.45948057	0.45688890	0.45533728	0.4510742 (17)
1.5	1.5	0.54930614	0.50513652	0.49006459	0.48331974	0.47972832	0.47758588	0.471726 (2)
2.0	0.0	0.41389271	0.42018005	0.42097629	0.42111147	0.42113891	0.42114428	0.421145 (6)
2.0	0.5	0.48795109	0.46429984	0.45622604	0.45257417	0.45061901	0.44945033	0.4462607 (10)
2.0	1.0	0.54202495	0.50046092	0.48641918	0.48016010	0.47683419	0.47485271	0.4694505 (18)
2.0	1.5	0.58515036	0.53158535	0.51333087	0.50520022	0.50088581	0.49831761	0.491323 (3)
2.0	2.0	0.62122666	0.55918707	0.53795845	0.52850379	0.52348906	0.52050483	0.5123870 (19)

TABLE VI. Residual entropy s , obtained by extrapolating $f_0^{(0,0)}(L)$ to the infinite-system limit.

B. Relation to other models

1. Dimer loop model

The FPL² model is a loop model which exhibits a two-dimensional manifold of fixed points in its phase diagram. Certain points in the critical region map to previously studied lattice models and here we comment on the relevance of our results for these models.

The dimer loop model studied by Raghavan *et al.* [15] is the $n_b = 2, n_g = 1$ FPL² model; see Fig. 1. The dimer loop model is defined by placing black and white dimers on the square lattice so that every vertex of the lattice is

covered by exactly one black and one white dimer. Every such configuration is given equal weight. The mapping to the FPL² model is achieved by identifying the bonds covered by dimers as making up the black loops, whilst the uncovered bonds form the grey loops. The original motivation for studying this dimer problem is that it leads to a height model with a two-component height; cfr. the traditional dimer model which is described by a single component height.

Performing Monte Carlo simulations of the dimer loop model Raghavan *et al.* reached the conclusion that one of the two height components is rough whilst the other one is “anomalously smooth”, i.e., its structure function decays at small wave-vectors \mathbf{q} slower than $1/\mathbf{q}^2$; a $1/\mathbf{q}^2$ dependence is to be expected in a Gaussian field theory.

In light of our results we would conclude that the dimer loop model is critical with a central charge $c = 2$. This follows from Eq. (6.4) for $n_b = 2$ and $n_g = 1$. The two components of the height found by Raghavan *et al.* should therefore both be rough, each contributing one to the central charge ($c = 1 + 1$). Furthermore, we believe that the observed anomalous behaviour of one of the heights can be attributed to the fact that this model is exactly at the boundary of the critical region of the FPL² model. We observe a similar effect in our numerical transfer matrix results which show largest deviations from the proposed exact formulae for loop fugacities at the critical-region boundary. The culprit might be logarithmic corrections due to the presence of marginal operators. To check this hypothesis and reconcile it with the fact that no such effects are seen in Monte Carlo simulations of the four-colouring model [28] ($n_b = n_g = 2$), which is also at the boundary of the critical region, simulations of the dimer-loop model for larger system sizes would be welcome.

2. Three-state Potts antiferromagnet

The critical ground state of three-state Potts antiferromagnet maps to the equal-weighted six-vertex model [16] which is the $n_b = n_g = 1$ point in the critical region of the FPL² model; see Fig. 1. Along the line $n_b = n_g$ the colouring representation of the FPL² model has the additional symmetry with respect to cyclic permutations of the four colours; see Sec. VC 2. This explains the origins of the \mathbf{Z}_4 symmetry found by Saleur for the *three-state* Potts antiferromagnet [56].

3. Folding model

The folding model of the square-diagonal lattice recently investigated by Di Francesco [57] maps onto a constrained version of the $(n_b, n_g) = (2, 2)$ FPL² model. The constraint consists in allowing only the vertices 1, 3, 5 and 6 of Fig. 3 for sites on the even sublattice, and similarly vertices 2, 4, 5 and 6 on the odd sublattice.

We have modified our transfer matrices to take this constraint into account. Our result for the folding entropy, $s = 0.4604(4)$, is in complete agreement with Ref. [57].⁷ Interestingly enough the finite-size scaling of the gaps in the eigenvalue spectrum seems to indicate that the model is not critical for general values of the loop fugacities. From the field theory of the FPL² model we should be able to understand why the constraint imposed by the folding model leads to a relevant perturbation which takes the system away from criticality. This we leave as an interesting open question. Incidentally, the situation is very reminiscent of the reformulation of the Q -state Potts model in terms of a staggered vertex model. Only at the critical point are the vertex weights on the even and odd sublattices identical, thus allowing for an exact solution of the model [32].

C. Conformal field theory

The Liouville field theory proposed for the effective theory of the FPL² model in the critical region is conformally invariant. Each point in the critical phase is characterised by the central charge and the scaling dimensions of primary fields, which are associated with electric and magnetic charges in the Coulomb gas. For generic values of the loop fugacities the background charge \mathbf{e}_0 is not commensurate with the electric charges that make up the lattice \mathcal{R}^* . This implies that amongst the electric operators there will be many (an infinite number, in fact) that have negative dimensions, signaling the non-unitary nature of the conformal field theory. Non-unitary CFT’s appear in many other critical geometrical models, critical percolation being the best known example.

Liouville field theory provides the Euclidean action for the Coulomb gas description of conformal field theories proposed by Dotsenko and Fateev [36]. As such it contains the so-called screening charges which are the vertex operators that make up the Liouville potential. In the original formulation these charges were introduced on formal grounds so as to ensure the existence of non-vanishing four-point correlation functions in the theory.

⁷Our normalisation is “per vertex” whilst that of Di Francesco is “per triangle”. Accordingly we find twice his result.

In order for these vertex operators not to disrupt the conformal symmetry of the modified Gaussian model (the modification is the addition of the boundary term to the gradient-square action) they are necessarily marginal, i.e., their scaling dimension is 2.

Here we have found a physical interpretation of the screening charges. Their rôle in loop models is to ensure that the number of large loops from scale to scale stays of order one; this translates into the statement that the loop fugacities do not flow under the action of the renormalisation group.

The fact that we have a concrete physical interpretation of the screening charges directly leads to the calculation of the elastic constants in the Liouville field theory. In the traditional Coulomb gas approach these coupling constants are calculated by comparing to formulae derived from an exact solution of the model. Once these constants are known marginal vertex operators that play the rôle of screening charges can be written down. Our construction basically reverses this procedure, and by doing so *makes no reference to an exact solution*.

Finally, we end with a speculative note concerning the prospects of solving the FPL² model via Bethe Ansatz. Namely, all loop models to date have been solved by this method after mapping them to a vertex model, following a procedure analogous to the one outlined in Sec. IV. This does not seem to work for the FPL² model, at least not along the $n_g = 1$ line [14]. Why this is so is an interesting open question.

One possibility is that the *full* FPL² model needs to be considered as opposed to the FPL model studied by Batchelor *et al.* for which $n_g = 1$ is fixed. A more intriguing possibility is that a Bethe Ansatz solution might be hindered (or made more difficult) by the non-trivial elasticity displayed by the FPL² model in its interface representation. This statement we base solely on the observation that all previously solved loop models are simple as interface models in the sense that the height fluctuations are described by a single elastic constant. For the FPL² model, as described in Sec. V, the stiffness tensor consists of three independent components. Whether indeed the interface representation of the loop model has any bearing on its Bethe Ansatz solvability remains to be seen.

ACKNOWLEDGMENTS

Useful discussions with M. Aizenman, J. L. Cardy, B. Duplantier, D.S. Fisher, C.L. Henley, T. Hwa, T. Prellberg, T. Spencer, F. Y. Wu, and C. Zeng are gratefully acknowledged. The authors would like to thank the Institute for Theoretical Physics at Santa Barbara, where this collaboration was initiated, for its warm hospitality. This research was supported in part by the Engineering and Physical Sciences Research Council under Grant

GR/J78327, and by the National Science Foundation under Grant PHY94-07194, and DMS 9304580.

APPENDIX A: DIMENSIONS OF ELECTRIC AND MAGNETIC OPERATORS

We calculate the scaling dimensions of electric and magnetic operators in the Coulomb gas theory described by the action

$$S_{CG} = \frac{1}{2} \int d^2\mathbf{x} g_\alpha (\partial H^\alpha)^2 + \frac{i}{4\pi} \int d^2\mathbf{x} (\mathbf{E}_0 \cdot \mathbf{H}) \mathcal{R}, \quad (\text{A1})$$

where \mathcal{R} is the scalar curvature. We are interested in the situation when the height field is defined on a flat surface, in which case \mathcal{R} is zero everywhere except at the boundaries.

1. Electric charges

The scaling dimension $x(\mathbf{E})$, of the electric-type operator $\exp(i\mathbf{E} \cdot \mathbf{H}(\mathbf{x}))$, follows from the two-point function

$$\left\langle e^{i\mathbf{E} \cdot \mathbf{H}(\mathbf{x})} e^{-i(\mathbf{E} - 2\mathbf{E}_0) \cdot \mathbf{H}(\mathbf{y})} \right\rangle \sim |\mathbf{x} - \mathbf{y}|^{-2x(\mathbf{E})}, \quad (\text{A2})$$

where the expectation value is with respect to the measure defined by the action S_{CG} . The extra electric charge $2\mathbf{E}_0$ appears due to the charged boundary conditions enforced by the curvature term in the Coulomb gas action, Eq. (A1).

We break up the calculation into two parts. First we calculate the two-point function, Eq. (A2), in the absence of the background charge ($\mathbf{E}_0 = 0$). We make use of the property of Gaussian integrals,

$$\left\langle e^{i\mathbf{E} \cdot \mathbf{H}(\mathbf{x})} e^{-i\mathbf{E} \cdot \mathbf{H}(\mathbf{y})} \right\rangle = \exp\left(-\frac{1}{2}(E_\alpha)^2 \langle (H^\alpha(\mathbf{x}) - H^\alpha(\mathbf{y}))^2 \rangle\right), \quad (\text{A3})$$

and of the known propagator for the massless scalar field in two dimensions (where we have dropped the regulators at large and small distances),

$$\langle (H^\alpha(\mathbf{x}) - H^\alpha(\mathbf{y}))^2 \rangle = \frac{1}{\pi g_\alpha} \ln |\mathbf{x} - \mathbf{y}|. \quad (\text{A4})$$

Combining the above two equations and comparing the result to Eq. (A2), we find

$$2x_e^{(0)}(\mathbf{E}) = \frac{1}{2\pi g_\alpha} (E_\alpha)^2; \quad (\text{A5})$$

the superscript (0) is there to remind us that this formula is valid only for $\mathbf{E}_0 = 0$.

This result for the two-point function can be rewritten as

$$\left\langle e^{i\mathbf{E}\cdot\mathbf{H}(\mathbf{x})} e^{-i\mathbf{E}\cdot\mathbf{H}(\mathbf{y})} \right\rangle = \exp[\mathcal{E}_{\mathbf{E}}^{(0)}(\mathbf{x}, \mathbf{y})], \quad (\text{A6})$$

where

$$\mathcal{E}_{\mathbf{E}}^{(0)}(\mathbf{x}, \mathbf{y}) = -\frac{1}{2\pi g_{\alpha}} (E_{\alpha})^2 \ln |\mathbf{x} - \mathbf{y}| \quad (\text{A7})$$

is the energy for two (vector) electric charges interacting via the two-dimensional Coulomb force; in this language $S_{\mathbf{E}}$ is the energy of the electrostatic field set up by the electric charges $\pm\mathbf{E}$, expressed in terms of the electrostatic potential \mathbf{h} . This seemingly trivial rewriting makes the calculation of $x(\mathbf{E})$, the electric dimension in the presence of a background charge, physically transparent.

To properly take into account the curvature term we define the height field over a disc of radius R , instead of the infinite plane, keeping in mind that at the end of the calculation we need to take the limit $R \rightarrow \infty$. In the case of the disc $\mathcal{R} = 8\pi\delta(R)$, and the curvature term introduces a charge $-2\mathbf{E}_0$ at the disc boundary. Therefore, the vacuum of the modified Coulomb gas must contain a *floating charge* $+2\mathbf{E}_0$ in the disc interior, and the electrostatic energy of this charged vacuum is $\mathcal{E}_{2\mathbf{E}_0}^{(0)}(0, R) = -4E_{0\alpha}^2 \ln(R)/2\pi g_{\alpha}$. Now, to find the scaling dimension of a vertex operator of charge \mathbf{E} , we imagine placing charges $+\mathbf{E}$ and $-\mathbf{E}$ at points \mathbf{x} and \mathbf{y} in the disc interior, and we calculate the total electrostatic energy with respect to the charged vacuum. The floating charge being positive will coalesce with the negative charge $-\mathbf{E}$. Using Coulombs law, Eq. (A7), we then calculate the interaction energy of charges $+\mathbf{E}$ at \mathbf{x} , $-\mathbf{E} + 2\mathbf{E}_0$ at \mathbf{y} , and $-2\mathbf{E}_0$ at R , keeping in mind $R \gg |\mathbf{x} - \mathbf{y}|$. The final result

$$\mathcal{E}_{\mathbf{E}}(\mathbf{x}, \mathbf{y}) = -\frac{1}{2\pi g_{\alpha}} E_{\alpha} (E_{\alpha} - 2E_{0\alpha}) \ln |\mathbf{x} - \mathbf{y}| \quad (\text{A8})$$

is obtained after the energy of the charged vacuum is subtracted. Now it is a simple matter to read off the scaling dimension as the negative coefficient in front of the logarithm,

$$2x(\mathbf{E}) = \frac{1}{2\pi g_{\alpha}} E_{\alpha} (E_{\alpha} - 2E_{0\alpha}) . \quad (\text{A9})$$

This result can be derived in a more rigorous fashion by constructing the stress-energy tensor for the field theory S_{CG} and calculating its operator product with the vertex operator $\exp(i\mathbf{E}\cdot\mathbf{H})$ [36].

2. Magnetic charge

To calculate the magnetic dimension $x(\mathbf{M})$ we consider the ratio of partition functions,

$$Z_{>\mathbf{M}}(\mathbf{x}, \mathbf{y})/Z_{>} \sim |\mathbf{x} - \mathbf{y}|^{-2x(\mathbf{M})} . \quad (\text{A10})$$

$Z_{>\mathbf{M}}(\mathbf{x}, \mathbf{y})$ is the sum (path integral) over height configurations where a vortex and an antivortex, of topological charge $\pm\mathbf{M}$, are placed at positions \mathbf{x} and \mathbf{y} of the basal plane, whilst $Z_{>}$ is the unconstrained sum:

$$Z_{>} = \int \mathcal{D}\mathbf{H} \exp\left(-\frac{1}{2} \int d^2\mathbf{x} g_{\alpha} (\partial H^{\alpha})^2\right) . \quad (\text{A11})$$

Here we have dropped the curvature term since it does not affect correlation functions of magnetic operators.

We can use the electrostatic analogy once again. Namely, we consider the interaction energy between two topological defects, $\mathcal{E}_{\mathbf{M}}(\mathbf{x}, \mathbf{y})$. Since $Z_{>}$ is a Gaussian path integral, it follows that

$$Z_{>\mathbf{M}}(\mathbf{x}, \mathbf{y})/Z_{>} = \exp[\mathcal{E}_{\mathbf{M}}(\mathbf{x}, \mathbf{y})] , \quad (\text{A12})$$

where

$$-\mathcal{E}_{\mathbf{M}}(\mathbf{x}, \mathbf{y}) = \frac{g_{\alpha}}{2\pi} (M^{\alpha})^2 \ln |\mathbf{x} - \mathbf{y}| . \quad (\text{A13})$$

The above interaction energy is calculated as the Gaussian action of the the classical configuration of the height field, \mathbf{h}_c . \mathbf{h}_c solves the classical equations of motion (Laplace's equation) with boundary conditions dictated by the presence of topological defects at \mathbf{x} and \mathbf{y} [34]. The scaling dimension of a magnetic-type operator is then the coefficient in front of the logarithm in Eq. (A13),

$$2x(\mathbf{M}) = \frac{g_{\alpha}}{2\pi} (M^{\alpha})^2 . \quad (\text{A14})$$

APPENDIX B: ENUMERATION OF THE CONNECTIVITIES

The implementation of the transfer matrix (TM) for the FPL² model on a cylinder of width L and length M requires an enumeration of the possible connectivity states of the L points on the dangling edges of row M . Each of these L points can either

1. be connected by \mathcal{G}_M to one of the dangling edges of row 0 through a string of flavour $i = \text{b, g}$, or
2. be connected by \mathcal{G}_M to one and only one other point in row M through a loop segment of flavour $i = \text{b, g}$.

A suitable representation of this information is furnished by a double state vector

$$\begin{pmatrix} i_1^{\text{b}} i_2^{\text{b}} i_3^{\text{b}} \dots i_L^{\text{b}} \\ i_1^{\text{g}} i_2^{\text{g}} i_3^{\text{g}} \dots i_L^{\text{g}} \end{pmatrix}, \quad (\text{B1})$$

which we shall refer to as the *index representation*. The indices i_k^{b} ($k = 1, 2, \dots, L$) are defined as follows:

1. $i_k^b = i_l^b$ is a (non-unique) positive integer if and only if points k and l are interconnected through a black string.
2. $i_k^b = 0$ if and only if point k touches a grey string or loop segment.
3. $i_k^b = -1$ if and only if point k is connected to a dangling edge of row 0 through a black string.

A similar definition is true for the indices i_k^g provided that one reads “grey” instead of “black” and *vice versa*. Two index representations are said to be identical if they are so up to the arbitrariness of the choice of positive integers. Also note that if $i_k^b \neq 0$ we have $i_k^g = 0$ and conversely.

A restriction on those indices that take positive values follows from the fact that loops of the same flavour are not allowed to intersect. Namely, if $j < k < l < m$ the equalities $i_j^b = i_l^b$ and $i_k^b = i_m^b$ cannot both be true. So in addition to being pairwise these connectivities are also *well-nested* [45]. The same is true for the grey indices, whereas there are no such restrictions when both flavours are involved. Indeed, connectivity states with $i_j^b = i_l^b$ and $i_k^g = i_m^g$ are explicitly allowed by the last two vertices shown in Fig. 3.

In practice we are only interested in the first few eigenvalues of TMs having a definite number of strings of each flavour. The relevant sectors of the TM are denoted $\mathbf{T}^{(s_b, s_g)}$, where s_i is the number of strings of flavour $i = b, g$. The fully packing constraint means that we can only examine system sizes L that have the same parity as $s_b + s_g$. The various sectors have different physical interpretations and each requires a different enumeration of the connectivity states. Since the two flavours enter at an equal footing in the partition function, Eq. (9.1), we only need consider $s_b \geq s_g$. The $\mathbf{T}^{(0,0)}$ sector contains information about the free energy and the energy-like correlation length. The geometrical scaling dimensions x_1 and x_2 can be obtained from the $\mathbf{T}^{(1,1)}$ and the $\mathbf{T}^{(2,0)}$ sectors respectively. Finally the sector $\mathbf{T}^{(1,0)}$ gives the scaling dimension of the twist-like operator.

Whilst the index representation contains all information necessary for determining the value of a given entry in the TM it is obviously not suitable for labeling the entries. We therefore need another representation, the so-called *number representation*, in which the connectivities are labeled by the integers $1, 2, \dots, C_L^{(s_b, s_g)}$, where $C_L^{(s_b, s_g)}$ is the number of different connectivity states in

the relevant sector. The practical implementation of the TMs relies on the mapping from the index to the number representation and its inverse.

We shall now consider, one by one, the various sectors of the TM.

1. $\mathbf{T}^{(0,0)}$ sector

When no strings are present all the L dangling edges of row M are pairwise connected with either a black or a grey loop segment. In particular L must be even. For any particular connectivity we can then decompose L as $L = 2p_b + 2p_g$, where $p_i \geq 0$ is the number of *pairs* of dangling edges covered by a flavour i loop segment. Since loops of different flavours are allowed to cross (see Fig. 3) the total number of connectivities is

$$C_L^{(0,0)} = \sum_{L=2p_b+2p_g} \binom{L}{2p_b} c_{p_b} c_{p_g}, \quad (\text{B2})$$

where c_p is the number of pairwise well-nested connectivities of $2p$ points. The c_p 's were first considered in the context of the Potts model [45], but were also found to play a central rôle in the TM formulation of the $O(n)$ model [47]. We shall now briefly recall how they are evaluated.

Consider a well-nested pairwise connectivity of $2p$ points given by the index representation $(i_1 i_2 \dots i_{2p})$. A recursion relation follows from observing that $i_1 = i_{2k}$ for precisely one integer $k \geq 1$. According to the well-nestedness criterion the sub-sequences $(i_2 i_3 \dots i_{2k-1})$ and $(i_{2k+1} i_{2k+2} \dots i_{2p})$ are both well-nested, and indices occurring in one of them do not occur in the other. Hence for $p \geq 1$

$$c_p = \sum_{k=1}^p c_{k-1} c_{p-k}, \quad (\text{B3})$$

and $c_0 = 1$. By means of the generating function $P(x) = \sum_{p=0}^{\infty} c_p x^p$ it is readily shown [47] that

$$c_p = \frac{(2p)!}{p!(p+1)!}, \quad (\text{B4})$$

and that asymptotically $c_p \sim 4^p$.

Using Eqs. (B2) and (B4) we can now compute explicit values for the $C_L^{(0,0)}$. These are shown for $2 \leq L \leq 16$ in Table VII.

L	4^L	$C_L^{(0,0)}$	$C_L^{(1,1)}$	$\tilde{C}_L^{(2,0)}$	L	$C_L^{(1,0)}$
2	16	2	2	1	1	1
4	256	10	24	12	3	6
6	4,096	70	300	150	5	50
8	65,536	588	3,920	1,960	7	490

10	1,048,576	5,544	52,920	26,460	9	5,292
12	16,777,216	56,628	731,808	365,904	11	60,984
14	268,435,456	613,470	10,306,296	5,153,148	13	736,164
16	4,294,967,296	6,952,660	147,232,800	73,616,400	15	9,202,050

TABLE VII. The number $C_L^{(s_b, s_g)}$ of FPL² connectivity states for L dangling edges accommodating s_i strings of flavour $i = b, g$. Only values of L with the same parity as $s_b + s_g$ are shown. When more than one string of any flavour is present further restrictions than the well-nestedness criterion apply, as described in the text. Accordingly the number $\tilde{C}_L^{(2,0)}$ is merely a useful upper limit on the true $C_L^{(2,0)}$. The efficiency of writing the TMs in the connectivity basis can be appreciated by comparing $C_L^{(0,0)}$ to 4^L , the latter being the dimensions of the TM written in the conventional colour basis, where every dangling end is labeled independently by **A**, **B**, **C** or **D**.

For obvious reasons we shall call the function

$$\rho(i_1 i_2 \dots i_{2p}) = k \quad (2.5)$$

defined by $i_1 = i_{2k}$ the *cut function* of the index representation $(i_1 i_2 \dots i_{2p})$. A complete ordering of the well-nested sequences is now induced by applying the cut function first to the whole sequence, then recursively to its right and finally to its left part [45,47]. Accordingly, the mapping from the index to the number representation for a well-nested one-flavour connectivity is accomplished by

$$\sigma(i_1 i_2 \dots i_{2p}) = \begin{cases} 1 & \text{if } p \leq 1 \\ \sum_{l=1}^{k-1} c_{l-1} c_{p-l} + \sigma(i_2 \dots i_{2k-1}) & \\ + [\sigma(i_{2k+1} \dots i_{2p}) - 1] c_{k-1} & \text{otherwise,} \end{cases} \quad (2.6)$$

where the c_p are given by Eq. (B4).

To give a complete specification of the connectivity of any *one* flavour in the state (B1) we need to keep track of the positions of those indices that are zero. For a fixed number of z zero indices this is accomplished by the lexicographic ordering

$$\psi(i_1 i_2 \dots i_L) = \begin{cases} 1 & \text{if } L = 1 \text{ or } z = L \\ \psi(i_2 i_3 \dots i_L) & \text{if } i_1 \neq 0 \\ \binom{L-1}{z} + \psi(i_2 i_3 \dots i_L) & \text{if } i_1 = 0, \end{cases} \quad (2.7)$$

assigning the lowest value to the sequence with all the zeros accumulated to the right.

The number representation of the two-flavour state (B1) is now obtained by first ordering according to the number of indices i_k^b being zero, then lexicographically ordering the positions of these zero indices, and finally using the ordering (2.6), first on the well-nested subsequence of non-zero black indices and then on the corresponding grey subsequence. More precisely, the mapping from the index to the number representation in the $(s_b, s_g) = (0, 0)$ sector is given by

$$\phi^{(0,0)} \begin{pmatrix} \mathbf{i}^b \\ \mathbf{i}^g \end{pmatrix} = \sum_{k=p_b+1}^{L/2} \binom{L}{2k} c_k c_{L/2-k} \quad (2.8)$$

$$+ [\psi(\mathbf{i}^b) - 1] c_{p_b} c_{p_g} + [\sigma(\tilde{\mathbf{i}}^b) - 1] c_{p_b} + \sigma(\tilde{\mathbf{i}}^g),$$

where $\mathbf{i}^b = (i_1^b i_2^b \dots i_L^b)$ denotes the sequence of black indices and $\tilde{\mathbf{i}}^b$ the subsequence of the p_b pairs of non-zero indices (and, of course, similarly for the grey flavour).

The inversion of Eq. (2.9), so as to furnish a mapping from the number to the index representation, is straightforward if we know how to invert the functions σ and ψ . Details on this have already been given in Ref. [50].

B. $\mathbf{T}^{(1,0)}$ sector

In the case of one black string spanning the length of the cylinder the number of dangling edges in row M can be written as $L = 2p_b + 2p_g + 1$, where the p_i have the same meaning as above. In particular L must be odd.

The presence of *one* string of either flavour does not impose any additional restrictions on the connectivity states of the subsequence of positive indices of that flavour. Indeed, if the position of the string is given by $i_r^b = -1$ the non-zero subsequence of $(i_{r+1}^b \dots i_L^b i_1^b \dots i_{r-1}^b)$ is still well-nested, and the arguments given above apply. The number of connectivity states is therefore found by multiplying the L possible positions of the string by the number of $(s_b, s_g) = (0, 0)$ states of the remaining $L-1$ points

$$C_L^{(1,0)} = L C_{L-1}^{(0,0)}. \quad (2.9)$$

Explicit values are shown in Table VII.

Similarly the mapping from the index to the number representation is found by first ordering after the position r of the string, and then after the value of $\phi^{(0,0)}$ taken of the remaining indices

$$\phi^{(1,0)} \begin{pmatrix} i_1^b i_2^b \dots i_L^b \\ i_1^g i_2^g \dots i_L^g \end{pmatrix} = (r-1) C_{L-1}^{(0,0)} \quad (2.10)$$

$$+ \phi^{(0,0)} \begin{pmatrix} i_1^b \dots i_{r-1}^b i_{r+1}^b \dots i_L^b \\ i_1^g \dots i_{r-1}^g i_{r+1}^g \dots i_L^g \end{pmatrix}.$$

C. $\mathbf{T}^{(1,1)}$ sector

When one string of each flavour is present $L = 2p_b + 2p_g + 2$ must be even, and again it suffices to augment the considerations from the $\mathbf{T}^{(0,0)}$ case by some book-keeping as to the positions of the two strings. Explicit values of

$$C_L^{(1,1)} = L(L-1)C_{L-2}^{(0,0)}. \quad (2.11)$$

are shown in Table VII.

Letting r_i denote the position of the string of flavour $i = b, g$ we find that

$$\begin{aligned} \phi^{(2,0)} \left(\begin{array}{c} \mathbf{i}^b \\ \mathbf{i}^g \end{array} \right) &= [(r_b - 1)(L - 1) + (|r_g - r_b| - 1)] C_{L-2}^{(0,0)} \\ + \phi^{(0,0)} \left(\begin{array}{c} i_1^b \dots i_{r_b-1}^b i_{r_b+1}^b \dots i_{r_g-1}^b i_{r_g+1}^b \dots i_L^b \\ i_1^g \dots i_{r_b-1}^g i_{r_b+1}^g \dots i_{r_g-1}^g i_{r_g+1}^g \dots i_L^g \end{array} \right) \end{aligned} \quad (2.12)$$

is the desired mapping from the index to the number representation.

A possible configuration of the system for $(s_b, s_g) = (1, 1)$ is illustrated in Fig. 8, where the index representation of the connectivity state for each completed row is shown to the right of the figure.

D. $\mathbf{T}^{(2,0)}$ sector

Considering now the case of two black strings, it appears that the number of connectivity states for L even is given by

$$\tilde{C}_L^{(2,0)} = \binom{L}{2} C_{L-2}^{(0,0)}, \quad (2.13)$$

where we have simply divided Eq. (2.11) by 2 to take into account the indistinguishability of two strings of the *same* flavour. This is however not quite true, since for $L \geq 4$ the number (2.13) includes certain disallowed basis states. For $L = 4$ these are

$$\begin{pmatrix} -1 & 1 & -1 & 1 \\ 0 & 0 & 0 & 0 \end{pmatrix} \text{ and } \begin{pmatrix} 1 & -1 & 1 & -1 \\ 0 & 0 & 0 & 0 \end{pmatrix}. \quad (2.14)$$

The reason why these states are not valid is that, by definition of the allowed vertices (see Fig. 3), black loop segments cannot cross a black string. In general, therefore, any configuration where the positions of two equal, positive black indices are separated by exactly one black string is not a valid one, even though the positive indices of each flavour satisfy the well-nestedness criterion. Accordingly, the true $C_L^{(2,0)}$ is less than the $\tilde{C}_L^{(2,0)}$ of Eq. (2.13).

We have not found it worthwhile to pursue the solution of this complication, since the numbers $\tilde{C}_L^{(2,0)}$ are already less than the $C_L^{(1,1)}$, and we need to diagonalise the transfer matrices $\mathbf{T}^{(1,1)}$ and $\mathbf{T}^{(2,0)}$ for the same values

of L in order to determine the scaling dimensions x_1 and x_2 with the same numerical precision. Instead we found it efficient to construct all the $\tilde{C}_L^{(2,0)}$ basis states, list the number representations of those that are disallowed, and force the corresponding entries of $\mathbf{T}^{(2,0)}$ to zero.

With this proviso the mapping from the index to the number representation is

$$\begin{aligned} \phi^{(2,0)} \left(\begin{array}{c} \mathbf{i}^b \\ \mathbf{i}^g \end{array} \right) &= [\psi(\mathbf{i}^b + \mathbf{1}) - 1] C_{L-2}^{(0,0)} \\ + \phi^{(0,0)} \left(\begin{array}{c} i_1^b \dots i_{r_1-1}^b i_{r_1+1}^b \dots i_{r_2-1}^b i_{r_2+1}^b \dots i_L^b \\ i_1^g \dots i_{r_1-1}^g i_{r_1+1}^g \dots i_{r_2-1}^g i_{r_2+1}^g \dots i_L^g \end{array} \right), \end{aligned} \quad (2.15)$$

where r_1 and r_2 are the positions of the two black strings, and $\psi(\mathbf{i}^b + \mathbf{1})$ means that we should lexicographically order the positions of the black indices that are -1 .

-
- [1] P.-G. de Gennes, *Scaling Concepts in Polymer Physics* (Cornell University Press, Ithaca, 1979).
 - [2] B. Nienhuis, Phys. Rev. Lett. **49**, 1062 (1982).
 - [3] B. Duplantier and H. Saleur, Phys. Rev. Lett. **59**, 539 (1987).
 - [4] C. J. Camacho and D. Thirumalai, Phys. Rev. Lett. **71**, 2505 (1993).
 - [5] H. S. Chan and K. A. Dill, Macromolecules **22**, 4559 (1989).
 - [6] B. Nienhuis, in *Phase Transitions and Critical Phenomena*, edited by C. Domb and J. L. Lebowitz (Academic, London, 1987), Vol. 11.
 - [7] J. Kondev, Phys. Rev. Lett. **78**, 4320 (1997).
 - [8] A. A. Belavin, A. M. Polyakov, and A. B. Zamolodchikov, Nucl. Phys. **B241**, 333 (1984).
 - [9] *Conformal Invariance and Applications to Statistical Mechanics*, edited by C. Itzykson, H. Saleur and J. -B. Zuber (World Scientific, Singapore, 1988).
 - [10] H. G. Evertz, *The loop algorithm*, cond-mat/9707221, and references therein.
 - [11] M. Aizenman and B. Nachtergaele, Commun. Math. Phys. **164**, 17 (1994).
 - [12] J. T. Chalker and P. D. Coddington, J. Phys. C **21**, 2665 (1988).
 - [13] D.-H. Lee, Phys. Rev. B **50**, 10788 (1994).
 - [14] M. T. Batchelor, H. W. J. Blöte, B. Nienhuis and C. M. Yang, J. Phys. A **29**, L399 (1996).
 - [15] R. Raghavan, C. L. Henley, and S. L. Arouh, J. Stat. Phys. **86**, 517 (1997).
 - [16] H. Park and M. Widom, Phys. Rev. Lett. **63**, 1193 (1989).
 - [17] J. Basile, T. Garel and H. Orland, J. Phys. A: Math. Gen. **25**, L1323 (1992).
 - [18] B. Duplantier in *Fundamental Problems in Statistical Mechanics VII*, edited by H. van Beijeren (North-Holland, Amsterdam, 1990).
 - [19] H. W. J. Blöte and B. Nienhuis, Phys. Rev. Lett. **72**, 1372 (1994).

- [20] M. T. Batchelor, J. Suzuki and C. M. Yung, Phys. Rev. Lett. **73** 2646 (1994).
- [21] J. Kondev, J. deGier and B. Nienhuis, J. Phys. A **29**, 6489 (1996).
- [22] D. A. Huse and A. D. Rutenberg, Phys. Rev. B **45**, 7536 (1992).
- [23] B. Duplantier and H. Saleur, Nucl. Phys. B **290**, 291 (1987).
- [24] H. Orland, C. Itzykson and C. de Dominicis, J. Phys. (Paris) **46**, L353 (1985).
- [25] A. L. Owczarek, T. Prellberg and R. Brak, Phys. Rev. Lett. **70**, 951 (1993).
- [26] T. G. Schmalz, G. E. Hite and D. J. Klein, J. Phys. A: Mat. Gen. **17**, 445 (1984).
- [27] S. Higuchi, *Field theoretic approach to the counting problem of Hamiltonian cycles of graphs*, cond-mat/9711152. To appear in Phys. Rev. E.
- [28] J. Kondev and C. L. Henley, Phys. Rev. B **52**, 6628 (1995).
- [29] N. Read in *Proceedings of the Kagomé Workshop*, edited by P. Chandra (NEC Laboratories, Princeton, 1992).
- [30] J. L. Cardy, Nucl. Phys. B **419**, 411 (1994).
- [31] A. Trovato and F. Seno, Phys. Rev. E **56**, 131 (1997).
- [32] R. J. Baxter, *Exactly Solved Models in Statistical Mechanics* (Academic Press, New York, 1982).
- [33] J. Cardy in *Fields, Strings and Critical Phenomena*, edited by E. Brezin and J. Zinn-Justin (North-Holland, Amsterdam, 1990).
- [34] P. M. Chaikin and T.C. Lubensky, *Principles of condensed matter physics* (Cambridge University Press, Cambridge, 1995); chapter 9.
- [35] M. Aizenman, Nucl. Phys. **B485**, 551 (1997).
- [36] V.I. S. Dotsenko and V. A. Fateev, Nucl. Phys. B **240**, 312 (1984); *ibid.* **251**, 691 (1985).
- [37] H. W. Blöte, J. L. Cardy and M. P. Nightingale, Phys. Rev. Lett. **56**, 742 (1986); I. Affleck, Phys. Rev. Lett. **56**, 746 (1986).
- [38] J. L. Cardy, J. Phys. A **16** L355 (1983).
- [39] J. Kondev and C. L. Henley, Phys. Rev. Lett. **74**, 4580 (1995).
- [40] H. Saleur and B. Duplantier, Phys. Rev. Lett. **58**, 2325 (1987).
- [41] P. Ginsparg in *Fields, Strings, and Critical Phenomena*, edited by E. Brézin and J. Zinn-Justin (North Holland, Amsterdam, 1989).
- [42] A. Kast, J. Phys. A: Math. Gen. **29**, 7041 (1996).
- [43] S. T. Chui and J. D. Weeks, Phys. Rev. B **14**, 4978 (1976). J. V. José, L. P. Kadanoff, S. Kirkpatrick, and D. R. Nelson, Phys. Rev. B **16**, 12 (1977).
- [44] R. J. Baxter, J. Math. Phys. **11**, 784 (1970).
- [45] H. W. J. Blöte and M. P. Nightingale, Physica A **112**, 405 (1982).
- [46] J. Cardy and J. L. Jacobsen, Phys. Rev. Lett. **79**, 4063 (1997).
- [47] H. W. J. Blöte and B. Nienhuis, J. Phys. A **22**, 1415 (1989).
- [48] J. L. Cardy in *Phase Transitions and Critical Phenomena* Vol. 11, ed. C. Domb and J. L. Lebowitz (Academic Press, London, 1987).
- [49] S. L. A. de Queiroz, Phys. Rev. E **51**, 1030 (1995).
- [50] J. L. Jacobsen and J. Cardy, Nucl. Phys. B **515**, 701 (1998).
- [51] J. L. Cardy, J. Phys. A: Math. Gen. **19**, L1093 (1986).
- [52] E. H. Lieb, Phys. Rev. **162**, 162 (1967).
- [53] P. J. Flory, J. Chem. Phys. **10**, 51 (1942).
- [54] M. L. Huggins, J. Phys. Chem. **46**, 151 (1942).
- [55] P.W. Kasteleyn, Physica **29**, 1329 (1963). B. Duplantier, J. Stat. Phys. **49**, 411 (1987).
- [56] H. Saleur, Nucl. Phys. B **360**, 219 (1991).
- [57] P. Di Francesco, *Folding the square-diagonal lattice*, cond-mat/9803051.